Journal of Volcanology and Geothermal Research, 57 (1993) 193–217
Elsevier Science Publishers B.V., Amsterdam

High-Mg andesites from the southern termination of the New Hebrides island arc (SW Pacific)

M. Monzier[a,1], L.V. Danyushevsky[b,2], A.J. Crawford[c], H. Bellon[d] and J. Cotten[d]

[a]*UR 1F, ORSTOM, B.P. A5, Nouméa Cedex, New Caledonia*
[b]*Vernadsky Institut of Geochemistry, 19 Kosygin street, Moscow, 117975, Russia*
[c]*Geology Department, University of Tasmania, GPO Box 252C, Hobart, 7001 Tasmania, Australia*
[d]*Departement des Sciences de la Terre (GDR 910-GEDO), Université de Bretagne Occidentale, B.P. 452, 29275, Brest Cedex, France*

(Received December 8, 1992; revised version accepted June 18, 1993)

ABSTRACT

In the southern New Hebrides arc, magmatic and tectonic processes are closely linked. Between 21°S and 22°S, a "normal" broadly arc tholeiitic magmatic suite is essentially similar to those occurring in the main part of the arc, whereas south of 22°S, at the southern termination of the arc, a high-Mg andesite suite appears, with the more mafic endmembers having mineralogical and compositional affinities to high-Ca boninites. During the last 2 Ma, this southern termination propagated southwards and played a continuing role in the transient transform junction between the southern tip of the trench and the N–S spreading axis of the North Fiji Basin. In this region, which has been dominated for several million years by fast transform motions, the low magma production rates in this section of the arc, and the unusual boninite-related affinities of the arc volcanics may be due to a combination of a subducting slab torn by hinge zones, abnormally small depth-to-slab distances beneath volcanoes, and an unusually hot ambient geotherm due to rising diapirs supplying the intersecting back-arc spreading axis. The on-going collision between the Loyalty Ridge and the arc may also contribute to these unusual magmatic characteristics, as presently only a very small amount of convergence occurs along the southernmost segment of the trench.

In such a complex tectonic setting, with a spreading axis propagating into an intra-oceanic arc, and major transform plate motions, generation of high-Ca boninitic magmas occurs by melting of a refractory hydrated mantle at a shallow level under the Hunter Ridge, the necessary extra heat being supplied by the rising diapirs supplying magmas to the intersecting spreading ridge axis. The high-Mg andesite suite probably results via a combination of fractional crystallization from such high-Ca boninitic parental magmas and subsequent magma mixing processes, operative all along the southern termination of the arc.

1. Introduction

From approximately 12–10 Ma, clockwise rotation of the New Hebrides (NH) volcanic arc has been associated with both subduction of the Australasian plate and opening of the North Fiji Basin (Fig. 1; Auzende et al., 1988; Greene et al., 1988). In this region, the eastern edge of the Australasian plate is constituted by several small oceanic basins, island chains and submarine massifs: from north to south, these include the poorly-known Santa Cruz basin and West Torres massif, the D'Entrecasteaux Zone, a twin-ridged, arcuate submarine chain with uplifted Eocene oceanic crust and arc-related seamounts (Andrews, Packham et al., 1975; Maillet et al., 1983; Collot, 1989; Collot et al., 1992), the Eocene North Loyalty Basin (Andrews, Packham et al., 1975; Weissel et al., 1982; Collot et al., 1985), the massive, poorly

[1]Present address: ORSTOM, B.P. 76, Port-Vila, Vanuatu.
[2]Present address: Geology Department, University of Tasmania, GPO Box 252C, Hobart, 7001 Tasmania, Australia.

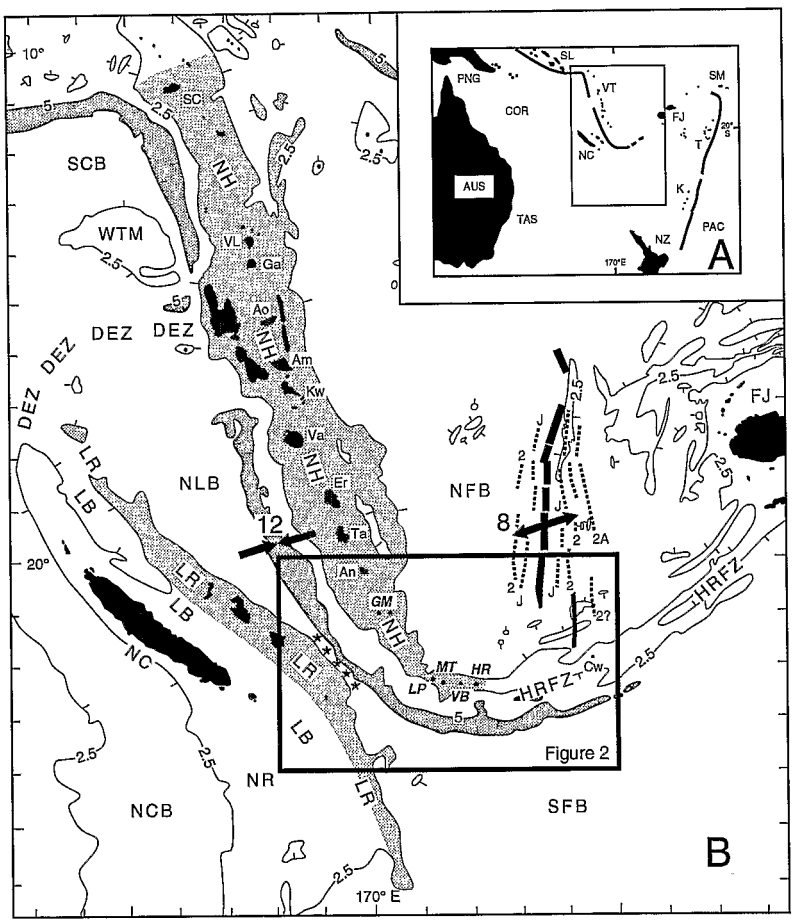

Fig. 1. Map of the Southwest Pacific (A) and outline map of the New Hebrides island arc (B). For (A): *PAC*=Pacific Ocean; *COR*=Coral Sea; *TAS*=Tasman Sea; *AUS*=Australia; *PNG*=Papua New Guinea; *SL*=Solomon islands; *VT*=Vanuatu; *NC*=New Caledonia; *FJ*=Fiji islands; *SM*=Samoa islands; *T*=Tonga islands; *K*=Kermadec islands; *NZ*=New Zealand. For (B): *NCB*=New Caledonia Basin; *NR*=Norfolk Ridge; *LB*=Loyalty Basin; *LR*=Loyalty Ridge; *NLB*=North Loyalty Basin; *DEZ*=D'Entrecasteaux Zone; *WTM*=West Torres Massif; *SCB*= Santa Cruz Basin; *NH*=New Hebrides islands; *SC*=Santa Cruz islands; *VL*=Vanua Lava; *Ga*=Gaua; *Ao*=Aoba; *Am*=Ambrym; *Kw*=Kuwae caldera; *Va*=Vate; *Er*=Erromango; *Ta*=Tanna; *An*=Anatom; *GM*=Gemini seamounts; *LP*=La Perouse seamount; *MT*=Matthew island; *VB*=Vauban seamount; *HR*=Hunter island; *Cw*=Conway reef; *HRFZ*=Hunter Fracture Zone; *SFB*=South Fiji Basin; *NFB*=North Fiji Basin. Dotted areas: New Hebrides trench (isobath 5 km), New Hebrides arc and Loyalty Ridge (isobath 2.5 km). Stars indicate the collision zone between LR and NH arc. Bathymetry from Kroenke et al. (1983). Convergence rate (in cm/yr) at the NH trench and divergence rate in the NFB from Louat and Pelletier (1989). Spreading axis and magnetic anomalies in the NFB from Auzende et al. (1988) and Maillet et al. (1989). The area covered by Fig. 2 is marked by a rectangle.

known Loyalty Ridge (Collot et al., 1982; Monzier et al., in prep.) and the Oligocene South Fiji Basin (Davey, 1982).

The flexure and subduction of such a composite plate has had a significant influence on the geodynamic evolution of the New Hebrides subduction zone. Ridge–arc or massif–arc collisions have played an increasingly important role in the tectonic and magmatic evolution of the New Hebrides arc (Daniel et al., 1986; Collot, 1989; Collot et al., 1989, 1992; Monzier et al., 1989, 1990, in prep.; Greene et al., in press). Complex multi-stage back-arc basin opening of the North Fiji Basin, and in-

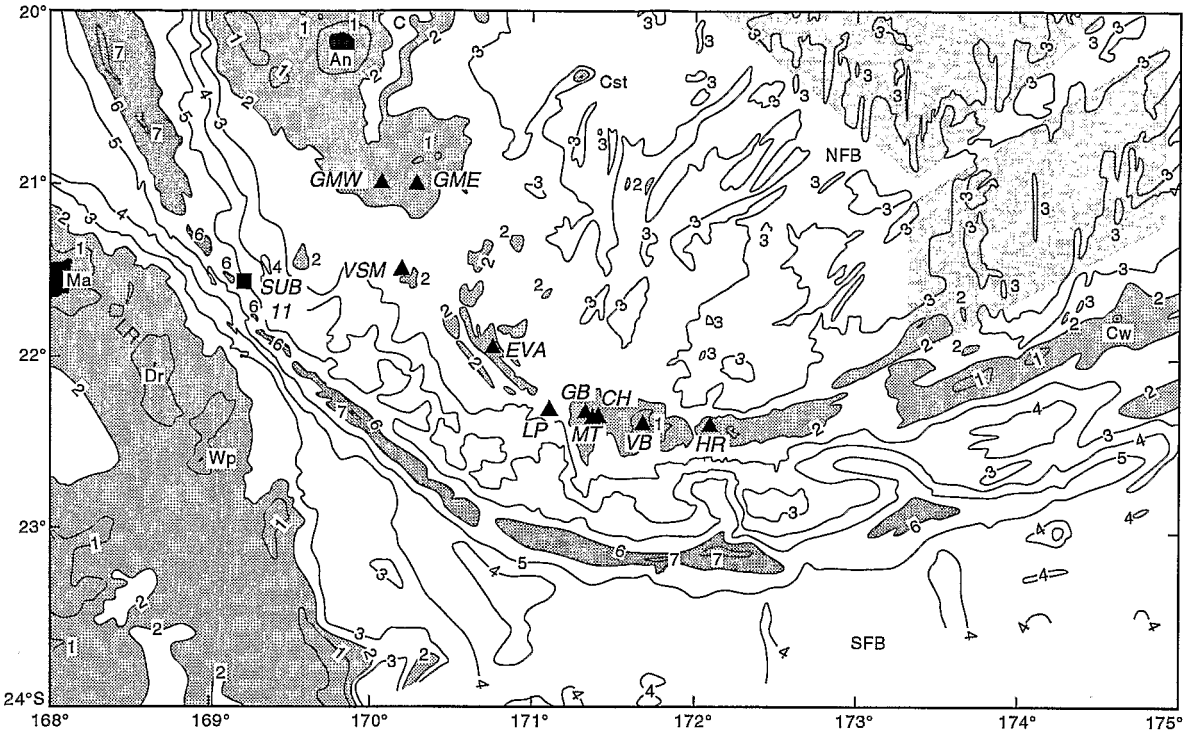

Fig. 2. Map of the southern part of the New Hebrides arc and North Fiji Basin. Bathymetry in km from Monzier et al. (1992). Dotted areas: NH trench (depths > 6 km), New Hebrides arc and Loyalty Ridge (depths < 2 km); light dotted area represents the 2 Ma to present oceanic crust generated in the North Fiji Basin (Auzende et al., 1988; Maillet et al., 1989). Abbreviations as for Fig. 1, with addition of: *Ma*=Mare island; *Dr*=Durand reef; *Wp*=Walpole; *C*=Coriolis troughs; *Cst*=Constantine bank. Volcanoes studied herein: *GMW*=Western Gemini seamount (sm); *GME*=Eastern Gemini sm; *VSM*=Volsmar sm; *SUB 11*=SUBPSO 11 Nautile dive locality; *EVA*=Eva sm; *LP*=La Perouse sm; *GB*=Gilbert sm; *MT*=Matthew island; *CH*=Charlotte sm; *VB*=Vauban sm; *HR*=Hunter island.

tra-arc or back-arc extensional tectonic troughs accompanied the rotation of the arc (Auzende et al., 1988; Lafoy et al., 1990; Recy et al., 1986, 1990; Charvis and Pelletier, 1989; Monjaret, 1989; Monjaret et al., 1991; Pelletier et al., 1993).

According to the quantitative model of Louat and Pelletier (1989), the present convergence rate along the nearly rectilinear N165°E part of the NH trench varies from 16 cm/yr (at 11°S) to 12 cm/yr (at 20°S), on an average N75°E azimuth. A minimum convergence rate occurs where the D'Entrecasteaux Zone collides with the central part of the arc (9 cm/yr). Oblique extension generally occurs along the eastern, back-arc flank of the main part of the NH arc, except at the latitude of the D'Entrecasteaux Zone collision zone, where back-arc compression is active. The North Fiji Basin presently shows an unusual pattern of opening, with several microplates bounded by spreading axes, extensional areas and transform faults. In the central part of the basin (16 and 21°S), a well established N–S spreading axis is active with an 8 cm/yr full spreading rate in a N72°E oblique direction (Fig. 1).

During rotation of the subduction zone, spreading in the North Fiji Basin led to southward lengthening of the trench–arc system from Anatom island to Hunter island (Falvey, 1978; Falvey and Greene, 1988; Louat et al., 1988). At the same time, this propagating southern termination of the arc has played a continuous role in the mobile transform junc-

tion between the southern tip of the trench and the spreading axis. Davey (1982) suggested that the southern New Hebrides trench may also coincide with an older crustal discontinuity (i.e. a former boundary between the oceanic crusts of North Loyalty and South Fiji Basin). Moreover, according to Monzier et al. (1990), the recent but developing collision between the 22°S salient of the Loyalty Ridge and the southern New Hebrides arc is producing a different tectonic evolution of the over-riding plate north and south of 22°S. At this latitude, an active E–W sinistral transform zone affects the arc and back-arc area (Fig. 3). North of this limit, near-orthogonal convergence is driven by active subduction of the oceanic lithosphere of the North Loyalty Basin. South of this boundary, oblique convergence has now stopped, only a very small amount of orthogonal (northward) convergence occurs at the trench (Fig. 3), and the Matthew–Hunter microplate is strongly coupled with the Australasian plate. A connection between this E–W sinistral transform zone and the 21°S sinistral offset of the North Fiji Basin spreading axis is probable (Fig. 3; Louat and Pelletier, 1989). Thus, at the present time, this area is unstable and transient, with considerable tectonic complexity (Maillet et al., 1989).

From the Santa Cruz islands at the northern end of the NH arc, to Anatom in the south, the main part of the ~1200-km-long NH arc trends N165°E, and includes a wide, massive and partly emergent volcanic ridge of complex history (Macfarlane et al., 1988; Katz, 1988; Greene et al., 1988). In this main part of the arc, Quaternary–Recent volcanoes of the Central Chain lie 100 to 200 km above a very steeply-dipping Benioff zone which in places reaches at least 350 km depth (Louat et al., 1988). Detailed petrological-geochemical studies of the NH arc volcanoes are currently in progress, but available data show that basalts and basic andesites are volumetrically dominant, with subordinate acid andesites and dacites (Macfarlane et al., 1988). Most of these rocks may be assigned to medium- to high-K "tholeiitic" series (using the criteria of Miyashiro (1974) and Gill (1981), who defined the "tholeiitic" series as having simply a high FeO^*/MgO value relative to SiO_2).

South of Anatom (Fig. 2), a major shortening of the Benioff zone occurs (Louat et al., 1988). The southern termination of the NH arc, including a section around 350 km long and with a sharp bend near La Perouse seamount, is narrow and almost totally submarine (except for the small active volcanic islands of Matthew and Hunter). Along this section of the arc, troughs on the eastern flank (i.e. back-arc) disappear and the volcanic chain is poorly developed, especially in front of the Loyalty–New Hebrides collision zone (Monzier et al., 1990, 1992). According to the model of Monzier et al. (1984), the dip of the Benioff zone decreases southward, with hinge zones tearing the downgoing slab. Thus, the Benioff zone lies at a depth of about 100 and 150 km beneath the twin Gemini seamounts (Fig. 2) and only about 85 km beneath Matthew and Hunter volcanoes; the latter are the only previously studied volcanoes of the southern termination of the NH arc (Maillet et al., 1986). Moreover, in contrast to the Central Chain arc volcanoes, Matthew and Hunter volcanoes are made up of medium-K broadly calc-alkaline acid andesites with unusually low TiO_2 contents (0.37–0.45% TiO_2 at 60–62% SiO_2 and 3–5% MgO).

2. The southern New Hebrides arc: new data

2.1. Volcanic edifices and sample locations

During the VOLSMAR and GEMINI cruises (R.V. "ALIS" of ORSTOM, 1989), sampling by dredging and scuba-diving was carried out on submarine volcanoes of the southern NH arc, aimed at recovering samples from along the almost unknown, 300 km-long submarine section of the arc. All volcanoes sampled are located on the crest of the submarine NH arc

platform (Figs. 2 and 3). Complementing this sample suite are several samples from previous fieldwork on Matthew and Hunter active volcanoes (Maillet et al., 1986; M. Monzier, unpublished data), as well as samples recovered during the SUBPSO 11 NAUTILE dive (ORSTOM SUBPSO 1 cruise, 1989) from a thick, horizontal sequence of coarse volcanic breccias from the lower inner wall of the trench (5320–4645 m depth) at the latitude of the "Loyalty / New Hebrides" collision zone (Monzier et al., 1989). Dredge, dive and sample locations are reported in Table 1.

From NW to SE, the following volcanoes were dredged (Figs. 2 and 3): Western Gemini seamount (GMW, top at −40 m, volume ≈150 km^3), Eastern Gemini (GME, −80 m, ≈100 km^3), Volsmar (VSM, −1400 m, ≈70 km^3), Eva (EVA, −1140 m, ≈0.1 km^3, from a swarm of small cones <1 km^3), La Pérouse

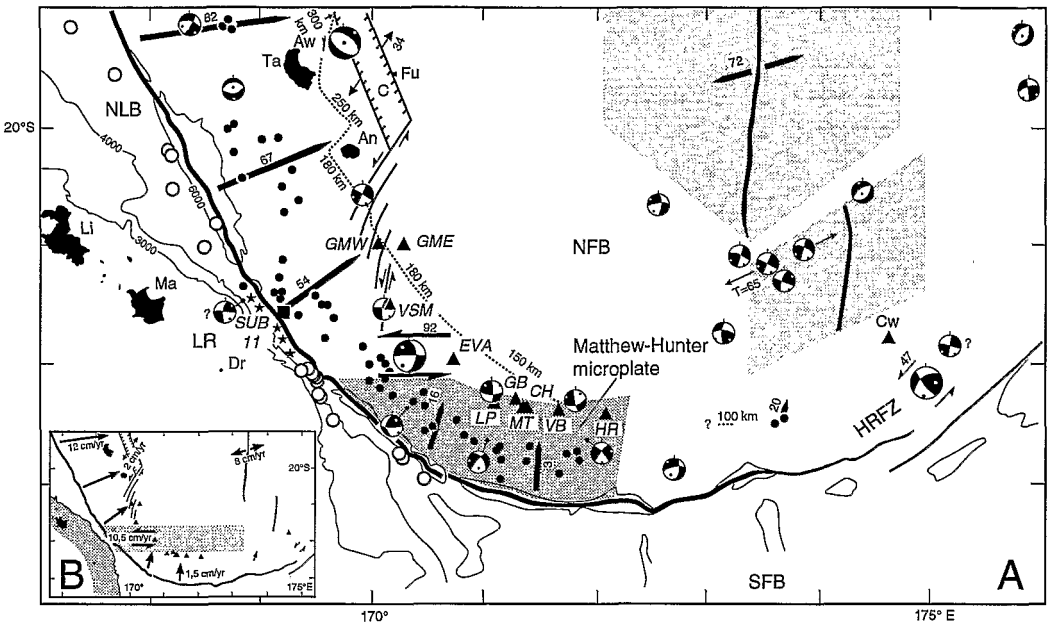

Fig. 3. Seismotectonics and present-day relative plate motions in the southern part of the New Hebrides arc and North Fiji Basin. (A) Simplified bathymetry (in m) from Monzier et al. (1992). Triangles represent the volcanoes studied herein. Abbreviations from Figs. 1 and 2, with addition of: *Li*=Lifou island; *Aw*=Aniwa; *Fu*=Futuna. Thick solid line=trench axis; stars indicate the Loyalty–New Hebrides collision zone; light dotted area represents the 2 Ma to present oceanic crust generated in the North Fiji Basin (cf. Fig. 2); dark dotted area=Matthew–Hunter microplate. Seismotectonics based on shallow (0–70 km) Centroid Moment Tensor (CMT) solutions (Dziewonski and Woodhouse, 1983; Dziewonski et al., 1983 to 1988; Giardini et al., 1985; and USGS/NEIC, 1987 to March 1990). New Hebrides subduction zone: ● =underthrust mechanism; large arrows=present-day relative convergent motion between the Australasian plate and the New Hebrides arc deduced from these underthrust solutions (with azimuth of the motion); ○=normal fault mechanism beneath the outer wall of the trench; focal sphere projections=normal fault and strike-slip mechanisms (big spheres represent several events); small double arrows=present-day N34°E extension within Coriolis trough, sinistral strike-slip motion at the southern termination of these troughs, and N20°E sinistral strike-slip motion under Gemini seamounts deduced from these solutions; large double arrows=present-day N92°E strike-slip motion across the NH arc, near 22°S; dotted line=projection of the eastern tip of the slab with depths in km. North Fiji Basin area: present-day N72°E accretion along the NFB spreading axis from Louat and Pelletier (1989); strike-slip mechanisms near the evolutionary transform zone (Maillet et al., 1989) joining, near 21°S, the two segments of the spreading axis indicate N65°E extensional motion. Hunter Fracture Zone: several strike-slip mechanisms indicate sinistral N47°E strike-slip motion along the HRFZ. (B) Present-day relative plate motions; rates are from Louat and Pelletier (1989). The sinistral E–W strike-slip zone which affects the arc in front of the Loyalty–New Hebrides collision zone is emphasized (Monzier et al., 1990).

TABLE 1

Locations and depths of dredges, dives and fieldwork localities on the volcanoes of the southern New Hebrides arc

	Type	From	to
Western Gemini			
GMW 50	Dr	20°59′1S/170°03′5E (−425 m)	20°59′7S/170°04′5E (−360 m)
GMW 54	Sc	21°00′7S/170°03′2E (−40 m)	
GMW 55	Dr	20°59′2S/170°01′9E (−710 m)	20°59′0S/170°02′7E (−560 m)
GMW 62	Sc	21°00′7S/170°03′2E (−40 m)	
Eastern Gemini			
GME 56	Dr	20°59′1S/170°15′7E (−630 m)	20°59′2S/170°16′9E (−260 m)
GME 59	Dr	20°59′9S/170°16′9E (−320 m)	20°59′9S/170°17′2E (−190 m)
GME 60	Dr	20°59′9S/17 0°16′6E (−190 m)	20°59′9S/170°16′8E (−80 m)
SUBPSO 11 dive			
SUB 1103	N	21°33′5S/169°12′6E (−5320 m)	
SUB 1105	N	21°33′3S/169°12′8E (−5032 m)	
SUB 1106	N	21°33′3S/169°12′8E (−5020 m)	
SUB 1111	N	21°32′8S/169°13′5E (−4645 m)	
Volsmar			
VSM 36	Dr	21°30′1S/170°10′1E (−1700 m)	21°30′0S/170°11′0E (−1400 m)
Eva			
EVA 35	Dr	21°59′3S/170°44′5E (−1500 m)	21°59′6S/170°45′8E (−1220 m)
La Pérouse			
LP 34	Dr	22°18′2S/171°06′0E (−1600 m)	22°18′1S/171°06′6E (−1130 m)
Gilbert			
GB 28	Dr	22°16′0S/171°17′2E (−1030 m)	22°16′4S/171°18′0E (−880 m)
GB 29	Dr	22°16′7S/171°17′2E (−800 m)	22°16′8S/171°17′6E (−650 m)
GB 30	Dr	22°17′0S/171°17′7E (−550 m)	22°17′0S/171°18′0E (−450 m)
GB 31	Dr	22°16′9S/171°17′4E (−440 m)	22°17′0S/171°17′6E (−380 m)
Matthew			
MTSM 25	Dr	22°22′8S/171°21′5E (−940 m)	22°22′4S/171°20′8E (−910 m)
MTSM 26	Dr	22°22′8S/171°21′4E (−980 m)	22°22′4S/171°20′7E (−915 m)
MT 1C, MT 11A, MT 14B, MT 20, MT 23B, MT 24C from Matthew island (Maillet et al., 1986)			
	FS	22°20′6S/171°21′2E (+177 m)	
Charlotte			
CH 19	Dr	22°20′0S/171°24′5E (−850 m)	22°20′1S/171°23′9E (−550 m)
CH 20	Dr	22°20′5S/171°23′5E (−500 m)	22°20′5S/171°23′5E (−460 m)
CH 22	Dr	22°20′2S/171°23′7E (−440 m)	22°20′2S/171°23′3E (−170 m)
Vauban			
VB 11	Dr	22°23′3S/171°43′6E (−1000 m)	22°24′0S/171°42′3E (−625 m)
VB 16	Dr	22°25′1S/171°40′7E (−500 m)	22°24′9S/171°41′2E (−420 m)
Hunter			
HR 1, HR 4B, HR 6, HR 8A, HR 9, HR 10, HR 11A, HR 12, HR 14, HR 15A, HR15B1, HR 15B2, HR 16, HR 17A, HR 18, HR 19, HR 20A, HR 20B, from Hunter island (HR 1 to HR 9: Maillet et al., 1986)			
	FS	22°23′6S/172°05′2E (+260 m)	

Dredge (Dr), scubadive (Sc), NAUTILE dive (N) or field sampling (FS). Navigation by GPS.

(LP, −1130 m, ≈35 km^3), Gilbert (GB, −265 m, ≈20 km^3), Matthew (MT, active, in solfataric stage, +177 m, ≈120 km^3, including Charlotte, see below), Charlotte (CH, an adventitious cone of Matthew, −37 m), Vauban (VB, −185 m, ≈240 km^3), and Hunter (HR, active, in solfataric stage, +260 m, ≈40 km^3). Volume estimates are maxima based on recent bathymetric data (Monzier et al., 1992). In comparison with Ambae (≈ 2500 km^3) or Ambrym (≈500 km^3) volcanoes in the central part of the arc (Fig. 1; bathymetric data from Chase and Seekins, 1988), all the studied volcanoes are medium- or small-sized volcanic

cones. However, Vauban seamount is unusually massive in contrast to the others in this arc segment and has an atypical, flat summit. Shallow water to mixed neritic-pelagic carbonate deposits capping the top of this volcano were dredged between 260 and 850 m depth.

2.2. Age of the volcanoes

Considering the recent evolution of the southern termination of the arc, it is probable that most of the sampled volcanoes are younger than 2 or 3 Ma. In fact, Matthew and Hunter are presently active volcanoes (Maillet et al., 1986), and K-Ar dating of samples VB11B and VB16A give ages of 0.8 and 1.1 Ma respectively, whereas sample SUB 1105 is younger than 1.4 Ma. However, biostratigraphical determinations on carbonate samples from the deposits capping Vauban seamount range from late Miocene to Plio-Quaternary in age and suggest that the end of the volcanic activity and the beginning of the subsidence of this volcano occurred during late Miocene–Pliocene times (L. Montaggioni, pers. commun., 1991). The apparently too-young K-Ar ages (<1.1 Ma) obtained for VB samples might be due to submarine weathering and Ar loss. Accordingly, Vauban seamount, with its unusual volume and peculiar shape, would be older than other volcanoes of this arc segment.

3. Petrography and mineral chemistry

Estimated modal phenocryst mineralogy for selected lavas is presented with whole-rock analyses in Table 2. Estimated vesicularity (vol.%) is highly variable, ranging from 0 to 75% (pumiceous samples). Phenocryst mineralogy of the sampled basalts, andesites and dacites (basalt $<$ 53% SiO_2 $<$ basic andesite $<$ 57% $<$ acid andesite $<$ 63% $<$ dacites $<$ 70 SiO_2%, with SiO_2 recalculated on an anhydrous basis; Gill, 1981) are typical of island-arc lavas (i.e. plagioclase dominant and subordinate ferromagnesian minerals), except for a few samples in which clinopyroxene and/or olivine are more abundant (LP 34B-C, CH 19D, VB 11C-16A). However, even plagioclase-dominated acid andesites from Hunter contain a few modal% of olivine phenocrysts.

Mineral compositions were obtained with a three spectrometer fully automated CAMECA SX50 electron microprobe at the University of Tasmania, using a wavelength-dispersive analytical system. Microprobe studies focused on the more basic lavas in the sample set, since one of our main aims was to identify the nature and affinities of the parent magma(s). A summary of the data is presented in Fig. 4A.

As described further on, compositional data indicate the existence of two broad magmatic groupings. The "normal" suite shows strong major-element similarities to the lavas erupted in the main NH arc Central Chain volcanoes, except for notably lower K_2O contents, whereas the "high-Mg" suite is characterized by lavas with significantly higher MgO contents at a given SiO_2 content, and has some boninitic affinities.

Samples GME 56C and SUB 1111, both belonging to the "normal" suite, show the classical mineralogy of arc-related lavas; 3% (by volume, vesicle-free) of An_{93-74} plagioclase phenocrysts, and subordinate augite and olivine (Fo_{77-75}) phenocrysts occur in basalt GME 56C (Table 2), whereas basic andesite SUB 1111 contains 4% An_{89-70}, 2% augite and endiopside (2 clearly distinct populations in the pyroxene quadrilateral) and rare orthopyroxene (En_{76-69}) phenocrysts.

Samples LP 34A, VB 11C and HR 11A all belong to the "high-Mg" andesite suite. LP 34A is a high-Mg basaltic andesite, petrographically and compositionally similar to LP 34B and C (Table 2). Endiopside-augite phenocrysts with magnetite inclusions are the dominant phenocryst phase in this rock (15%), followed by plagioclase (10% of An_{94-77}), and magnesian olivines (5% of Fo_{90-83}) that host two populations of Cr-spinels ($Cr\# = 100Cr/(Cr+Al) = 49–58$ and 74–78). VB 11C is an-

TABLE 2

Major-element compositions (wt.% summed to 100% volatile-free); $Fe_2O_3^*$ = total iron as Fe_2O_3; LOI = loss on ignition; Mg# determined on the basis of $Fe^{2+}/(Fe^{2+}+Fe^{3+})=0.9$. Trace elements in ppm. Estimated percentages for phenocryst phases resummed on the basis of 0% vesicles; x = rare (<1%)

Volcano	GMW	GMW	GME	GME	GME	SUB 11	SUB 11	VSM	VSM	EVA	EVA	EVA	LP	LP	GB	GB	MT	MT	MT	CH	CH	CH	VB	VB	HR	HR	HR	HR
Sample	55	54	56C	56A	60C	1111	1103	36A	36B	35A	35B	35D	34C	34B	29B	29C	11A	24C	SM25B	19D	22	19A1	16A	11C	11A	4B	10	16
wt%																												
SiO2	63.43	66.28	51.10	52.22	54.09	54.23	54.81	54.14	54.83	63.31	63.76	64.90	54.88	55.29	58.41	58.95	61.80	62.22	63.11	58.25	62.83	69.21	55.05	55.76	60.95	62.01	62.56	63.87
TiO2	0.64	0.57	0.85	1.05	1.31	0.93	0.96	0.65	0.82	0.64	0.58	0.63	0.59	0.58	0.66	0.66	0.45	0.42	0.44	0.49	0.41	0.52	0.78	0.67	0.50	0.49	0.56	0.38
Al2O3	15.50	15.18	19.10	16.21	14.90	15.32	15.53	18.70	16.65	14.51	14.17	14.85	14.19	13.95	15.88	16.40	15.16	15.51	15.73	14.85	16.07	14.35	14.02	13.66	14.97	15.10	15.04	15.37
Fe2O3*	7.30	6.00	10.12	11.94	12.80	11.71	11.23	9.88	11.64	6.77	6.67	6.55	8.43	8.14	7.81	7.70	6.33	6.12	5.99	7.62	6.14	4.24	8.52	8.62	6.10	6.03	5.88	5.51
MnO	0.15	0.14	0.17	0.21	0.22	0.18	0.18	0.16	0.19	0.11	0.11	0.10	0.15	0.15	0.13	0.13	0.11	0.11	0.10	0.13	0.10	0.09	0.14	0.14	0.10	0.10	0.10	0.09
MgO	2.11	1.58	4.50	5.07	4.35	4.53	4.36	3.11	3.27	3.42	3.59	2.25	8.72	8.54	5.09	4.25	4.47	3.99	3.15	5.64	3.20	1.17	7.83	8.77	5.74	5.25	4.43	3.81
CaO	5.82	4.96	11.61	10.27	8.68	9.39	8.24	9.88	8.54	6.21	6.14	5.29	9.60	9.77	7.67	7.37	6.91	6.80	6.05	8.96	6.38	3.22	8.13	7.97	6.69	6.56	6.75	6.35
Na2O	3.77	4.07	2.42	2.69	3.18	2.84	3.51	2.63	2.84	3.89	3.89	4.18	2.60	2.54	3.41	3.59	3.66	3.85	4.39	3.19	3.82	5.82	3.21	2.98	3.59	3.41	3.53	3.58
K2O	1.09	1.02	0.08	0.26	0.35	0.78	0.96	0.68	0.98	1.04	0.99	1.09	0.74	0.93	0.78	0.80	0.99	0.88	0.95	0.75	0.95	1.29	1.92	1.24	1.26	0.96	1.07	0.97
P2O5	0.20	0.20	0.05	0.08	0.12	0.10	0.21	0.15	0.25	0.10	0.10	0.15	0.10	0.12	0.15	0.15	0.10	0.08	0.08	0.10	0.08	0.10	0.41	0.20	0.10	0.08	0.08	0.08
LOI	0.40	0.30	0.37	-0.29	-0.42	1.67	1.91	0.33	0.43	1.05	0.87	0.65	0.45	0.50	0.00	0.06	0.08	0.12	1.12	0.46	0.52	2.45	0.42	0.44	0.46	-0.04	0.20	-0.10
Init. tot.	99.89	99.88	99.19	99.48	99.79	98.67	97.52	99.89	100.20	98.67	99.68	99.41	99.39	100.43	99.47	99.81	99.59	99.76	98.96	100.03	99.51	99.26	99.06	99.44	98.90	99.30	99.62	100.11
Mg#	39	37	49	48	43	46	46	41	38	53	54	43	69	70	59	55	61	59	54	62	53	38	67	69	67	66	62	60
ppm																												
Sc	21	19	37	42	42	31	28	28	31	22	23	19	33	34	30	29	23	23	21	32	21	13	28	28	22	22	23	23
V	125	75	300	330	460	329	364	320	350	165	165	167	235	230	275	285	150	145	145	180	155	50	270	260	175	155	145	175
Cr	2	2	38	30	4	13	2	17	10	59	79	14	339	347	130	68	94	74	30	185	29	2	260	306	190	201	124	73
Co	11	6	24	30	28	31	26	22	26	13	15	12	33	30	22	17	18	18	14	22	13	3	25	33	21	19	16	16
Ni	2	2	16	15	9	35	29	13	10	18	9	13	128	118	50	33	30	24	16	38	13	5	93	185	95	86	34	27
Cu	59	11	102	144	198	110	144	166	268	89	91	90	81	98	102	96	61	63	68	77	58	33	146	136	44	68	67	31
Zn	88	93	79	93	105	77	84	85	104	63	63	64	69	68	69	69	58	55	58	65	58	69	76	74	57	57	55	53
Rb	17	16	2	5	5	12	17	9	13	12	13	14	11	13	11	11	12	10	11	10	12	11	33	19	22	16	18	16
Sr	386	340	310	284	295	232	343	562	643	345	308	318	345	404	470	481	597	432	401	505	398	320	684	432	354	301	323	319
Y	27.0	29.0	18.0	23.0	29.0	23.4	21.5	16.1	20.0	19.5	18.0	19.5	13.3	13.2	15.8	15.8	13.3	12.7	13.2	12.4	12.7	19.0	27.0	18.0	12.8	11.7	10.8	11.2
Zr	66	69	31	41	60	51	48	41	63	111	109	122	54	57	78	79	99	73	86	68	84	119	188	110	83	72	48	72
Nb	<1,0	1.0	<1,0	<1,0	1.0	<1,0	<1,0	1.1	1.6	1.4	1.7	2.0	2.4	3.2	1.6	1.4	1.4	1.4	1.3	1.5	1.5	1.8	3.5	2.0	1.3	1.1	1.0	1.2
Ba	124	138	25	50	30	40	114	110	167	153	152	154	153	125	100	96	103	197	91	85	91	155	161	116	131	90	100	115
La	7.2	7.2	2.0	3.0	3.7	3.0	3.4	10.2	17.0	11.8	10.2	11.7	9.2	12.6	10.0	10.3	12.8	7.8	9.2	9.1	7.4	13.2	40.0	16.0	7.8	6.6	7.3	6.5
Nd	13.5	12.0	5.5	7.5	10.0	7.2	8.6	14.0	21.0	15.0	14.0	14.5	9.0	11.0	16.0	15.5	19.0	12.0	12.5	11.2	12.0	19.0	55.0	23.0	11.5	10.0	9.5	9.5
Eu	1.05	1.20	0.80	0.95	1.20	0.87	0.87	0.95	1.35	1.00	1.00	1.00	0.80	0.75	1.00	1.05	1.15	0.70	0.90	0.95	0.85	1.15	2.70	1.25	0.85	0.60	0.70	0.65
Dy	4.3	4.6	2.7	3.6	4.5	3.6	3.2	2.6	3.0	3.1	2.7	2.9	2.3	2.3	2.7	2.8	2.2	2.0	2.2	2.0	1.8	3.0	4.8	3.1	2.1	2.0	1.5	1.8
Er	2.9	2.8	2.1	2.5	3.1	2.1	2.0	1.9	2.3	2.2	2.1	2.1	1.5	1.5	1.9	2.0	1.6	1.6	1.4	1.5	1.7	2.2	2.8	2.2	1.6	1.3	1.3	1.4
Yb	2.55	2.85	1.80	2.20	2.75	2.32	2.23	1.60	1.80	1.80	1.85	1.85	1.20	1.30	1.50	1.50	1.25	1.25	1.40	1.20	1.30	1.75	2.05	1.55	1.25	1.20	1.00	1.20
PHENOCRYST MINERALOGY (est. vol.% on the basis of 0% vesicules)																												
Plg	10	12	3	3	2	4	2	30	20	12	10	10	10	10	25	25	21	28	28	7	25	12	10	5	20	23	20	22
Cpx	2	3	x	x	x	2	2	1	x	3	3	3	20	14	4	3	6	8	8	7	5	2	6	3	4	8	7	6
Opx	x	1				x				1	x	x			2	2	4	4	4	2	2	1	2	1	3	6	5	3
Fe-Ti Ox.	x	1					x	x	x	x	x	x			x	x	1	1	x	x	1	x	x		x	x	x	x
Ol	x	x	x	x	x			1	2	1	1		5	6		x	x	1					2	7	3	2	1	x
% Ves.	2	0	20	20	30	15	15	30	20	2	5	5	10	10	10	10	1	2	75	5	3	75	0	3	2	0	0	0

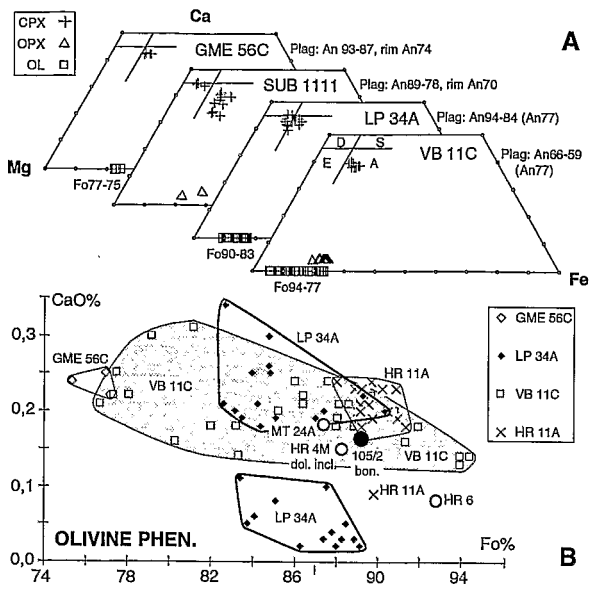

Fig. 4. Phenocryst and microphenocryst mineralogy of selected lavas. (A) Pyroxene quadrilateral showing compositional ranges for olivine, clinopyroxene and orthopyroxene in four selected lavas; the range for plagioclase is also indicated. (B) CaO% vs. Fo% for olivine phenocrysts; 105/2 bon. (●) = olivine phenocryst in a boninite from the Hunter Ridge near 173°E (Sigurdsson et al., 1993); MT 24A and HR 6 (○) = olivines from Matthew and Hunter andesites; HR 4M (○) = olivine in a doleritic inclusion from Hunter andesite (Maillet et al., 1986); abbreviations as in Fig. 2.

other high-Mg basaltic andesite (Table 2) with a quite distinct mineralogy: magnesian olivine phenocrysts (Fo_{94-77}; 7%) hosting Cr-spinels (Cr# = 71–82), An_{77-59} (5%), augite (3%), and orthopyroxene (En_{79-73}; 1%) with magnetite inclusions, coexist in this rock. Maillet et al. (1986) have reported a detailed mineralogical study of Matthew and Hunter high-Mg acid andesites, which are dominated by labradorite phenocrysts, and only a few analyses of magnesian olivine phenocrysts (Fo_{91-88}) from sample HR 11A (Table 2) have been added here.

The modal predominance of ferromagnesian minerals and the very forsteritic olivine phenocrysts in mafic rocks from the "high-Mg" series are unusual for arc lavas. Nevertheless, in spite of the broadly similar major element compositions of these rocks (Table 2), some significant differences exist in their phenocryst mineralogy. For example, phenocryst orthopyroxene is missing in LP 34A whereas it is present in VB 11C. Also, the modal abundance of clinopyroxene phenocrysts is considerably higher in LP 34A compared with VB 11C, and plagioclase and clinopyroxene phenocrysts are more calcic in this sample.

A plot of olivine phenocryst CaO versus Fo contents is given in Fig. 4B. Surprisingly, olivines from LP 34A have a restricted range in Fo content but plot in two quite distinct populations. The low CaO (0.02–0.11%) olivines are unlike those in all the other "high-Mg" series lavas, but have similar CaO contents to olivines in boninites (our unpubl. data). In addition, low-Ca olivines only include Cr-spinels with medium Cr# (49–58), which contrasts with the inferred boninitic affinities, since boninite chromites usually have Cr# > 75 (Crawford et al., 1989). These low-Ca olivines may be xenocrysts derived from spinel lherzolite or harzburgite upper mantle. Olivine phenocrysts from VB 11C define a single, broad population which shows a negative correlation between CaO and Fo contents, with CaO being around 0.13–0.14% in the most magnesian olivines (Fo_{94}). In both LP 34A and VB11C, the most calcic olivines are those included in pyroxenes. Olivines from the high-Ca population of LP 34A, VB 11C and HR 11A, plus additional olivines from Matthew and Hunter islands (MT 24A and HR 6, Maillet et al., 1986), all plot along the same trend and include Cr-rich spinels (Cr# = 71–82). Interestingly, olivines from a doleritic-textured cognate inclusion (HR 4M) with a high-Ca boninite composition from Hunter island (Maillet et al., 1986), and from a boninite (105/2) dredged along the Hunter Ridge (Sigurdsson et al., 1993) also plot along this trend and include Cr-rich spinels.

4. Whole-rock geochemistry

4.1. Analytical techniques

Major- and trace-element (V, Cr, Co, Ni, Cu, Zn, Rb, Sr, Ba) analyses of 76 selected lavas, 29 of which have complementary trace elements and REE (Sc, Y, Zr, Nb, La, Nd, Eu, Dy, Er, Yb) (Table 2), were carried out for this study. The complete set of data is available upon request (M.M.).

Selected rock fragments were ground in agate. Powders were digested with a concentrated acid mixture (1:8 HNO_3:HF). Fluorides were then dissolved and HF neutralized with an H_3BO_3 solution. International standards (JB2, BEN, ACE, GSN, MICA-Fe) were used for calibration. Major elements were determined by flame Atomic Absorption Spectrometry (AAS), Atomic Emission Spectrometry (AES) or Colorimetry (C): SiO_2 (AAS, relative standart deviation = 1%), TiO_2 (AAS, 5%), Al_2O_3 (AAS, 2%), Fe_2O_3 (AAS, 2%), MnO (AES, 5%), MgO (AAS, 2%), CaO (AAS, 2%), Na_2O (AAS, 2%), K_2O (AAS, 2%) and P_2O_5 (C, 10%). Trace elements were determined by AAS, AES or Inductively Coupled Plasma Emission Spectrometry (ICPES): Rb (AES, limit of detection in ppm = 1, relative standard deviation = 5%), Ba (AAS, 20, 10%), Nb (ICPES, 1, 5%), La (ICPES, 1, 5%), Sr (AES, 1, 5%), Nd (ICPES, 1, 5%), Zr (ICPES, 2, 5%), Eu (ICPES, 0.2, 5%), Dy (ICPES, 0.5, 5%), Y (ICPES, 0.5, 5%), Er (ICPES, 1, 10%), Yb (ICPES, 0.2, 5%), V (AAS, 20, 10%), Cr (AAS, 2, 5%), Co (AAS, 2, 5%), Ni (AAS, 2, 5%), Cu (AAS, 1, 5%), Zn (AAS, 2, 5%) and Sc (ICPES, 0.5, 5%). In this paper, major elements are always expressed as wt.%, recalculated to 100% volatile free.

4.2. Classification and comparison with other suites

The major-element geochemical variation of the lavas from the southern termination of the NH arc is presented in Figs. 5 and 6. These data are compared with:

(1) 204 unpublished analyses of lavas from the NH Central Chain (performed by the same laboratory, with the same analytical procedures as those reported here for lavas from the southern termination of the NH arc).

(2) 26 analyses of boninites from the north Tonga Ridge (Falloon and Crawford, 1991), and 2 analyses of boninites from the intersection of the southernmost North Fiji Basin spreading centre and the Hunter Ridge (Sigurdsson et al., 1993).

(3) 4 analyses of dolerite-textured boninite inclusions and 1 analysis of a pyroxene cumulate inclusion, in subaerial lavas from Matthew and Hunter volcanoes (Maillet et al., 1986).

(4) 8 analyses (1 basalt, 2 mafic andesites and 5 sodic rhyolites) of rocks from the intersection of the southernmost North Fiji Basin spreading centre and the Hunter Ridge (Sigurdsson et al., 1993).

(5) 25 analyses of BABB (Back-arc Basin Basalts) and MORB from the southernmost part of the North Fiji Basin and the Hunter Ridge (Eissen et al., 1991; Sigurdsson et al., 1993).

The lavas from the volcanoes at the southern termination of the NH arc show a compositional range from basalts to rhyolites (from 51 to 70% SiO_2), and clearly, a number of distinct magmatic suites can be identified from major- and trace-element data, sometimes even for rocks from the same volcano (e.g. Vauban). With the notable exception of two unusually K-rich basic andesites from Vauban Seamount (labelled VBHK in Figs. 5–10), all the analyzed lavas lavas are systematically lower in K_2O, at a given SiO_2 level, compared to recent lavas of the NH Central Chain volcanoes (Fig. 5). Classification into tholeiitic versus calc-alkaline is notoriously complicated for arc-related lavas. On a FeO*/MgO vs. SiO_2 diagram (Fig. 5), the lavas from the Gemini East seamount (GME), the forearc slope of

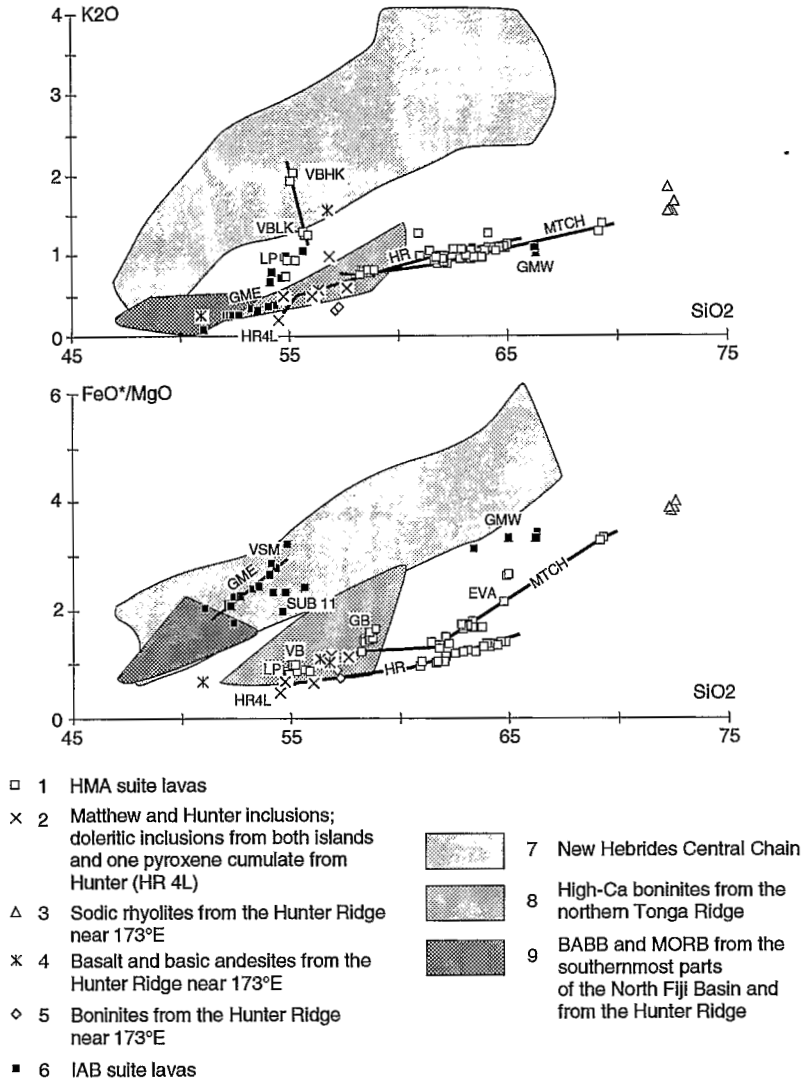

Fig. 5. K_2O% and FeO*/MgO vs. SiO_2% diagrams (all data recalculated to 100% volatile free); abbreviations as in Fig. 2. *1*: this study; *2*: from Maillet et al. (1986); *3*, *4* and *5*: from Sigurdsson et al. (1993); *6*: this study; *7*: 204 unpublished analyses of recent arc lavas from Vanua Lava, Aoba, Ambrym, Kuwae and Tanna (see Fig. 1 for location of these volcanoes); *8*: from Falloon and Crawford (1991); *9*: from Eissen et al. (1991) and Sigurdsson et al. (1993). 9*VBHK*=high-K Vauban seamount basaltic andesite; *VBLK*=low-K Vauban seamount basaltic andesite. Individual trends for Hunter (*HR*), Matthew and Charlotte (*MTCH*) and Eastern Gemini lavas (*GME*) are shown.

this region (SUB 11) and Volsmar seamount (VSM) show a broad tholeiitic trend (Gill, 1981). On a FeO* vs. FeO*/MgO plot, the lavas classified as tholeiitic above also define a broad but distinct Fe-enrichment trend, and may be classified as arc tholeiites. This suite of lavas shows, except for K_2O, strong compositional similarities to arc lavas from the main section of the New Hebrides arc (Fig. 5) and is therefore referred to as a "normal" island-arc basalt suite, herein abbreviated to IAB.

In contrast, basaltic andesites to rhyolites from the southernmost NH arc subaerial volcanoes and seamounts (south of 22°S) define

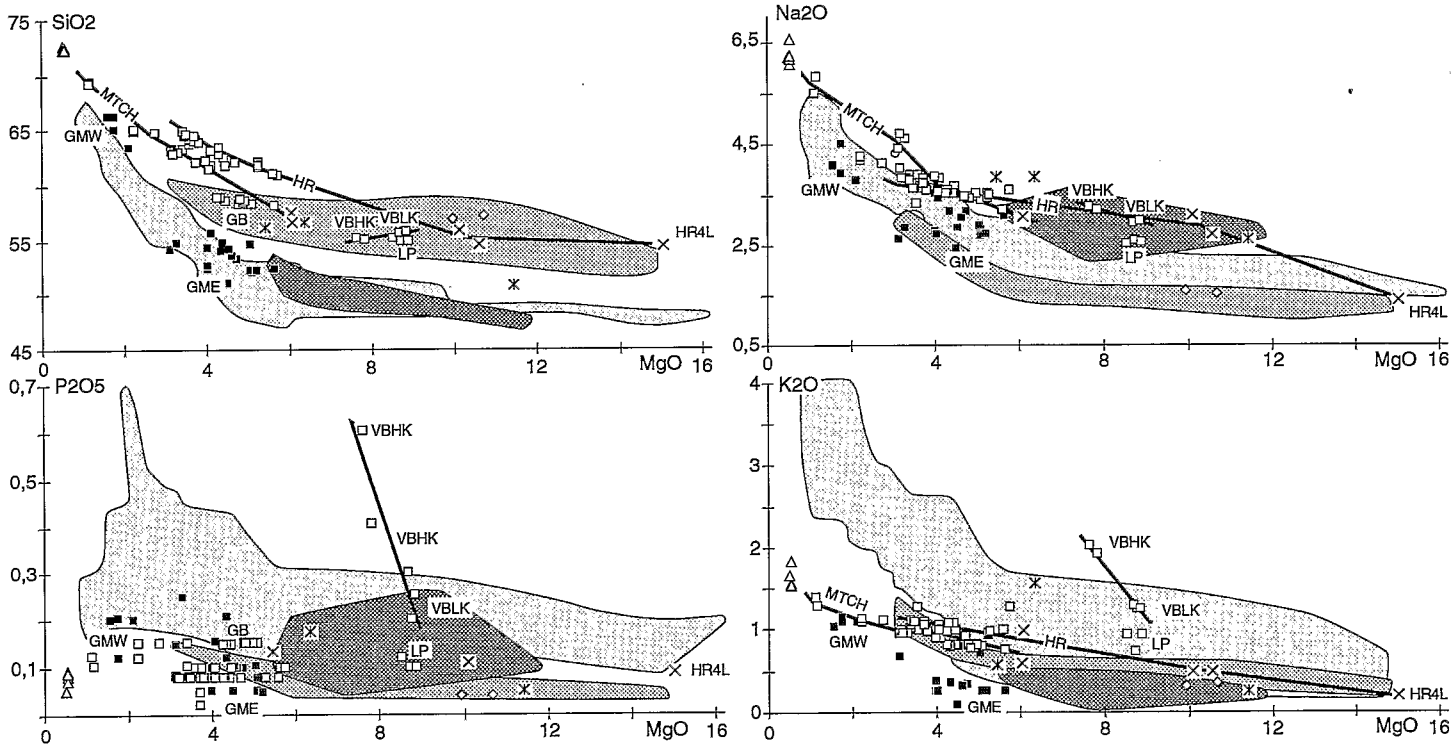

□ 1 HMA suite lavas

× 2 Matthew and Hunter inclusions; doleritic inclusions from both islands and one pyroxene cumulate from Hunter (HR 4L)

△ 3 Sodic rhyolites from the Hunter Ridge near 173°E

✳ 4 Basalt and basic andesites from the Hunter Ridge near 173°E

◇ 5 Boninites from the Hunter Ridge near 173°E

■ 6 IAB suite lavas

7 New Hebrides Central Chain

8 High-Ca boninites from the northern Tonga Ridge

9 BABB and MORB from the southernmost parts of the North Fiji Basin and from the Hunter Ridge

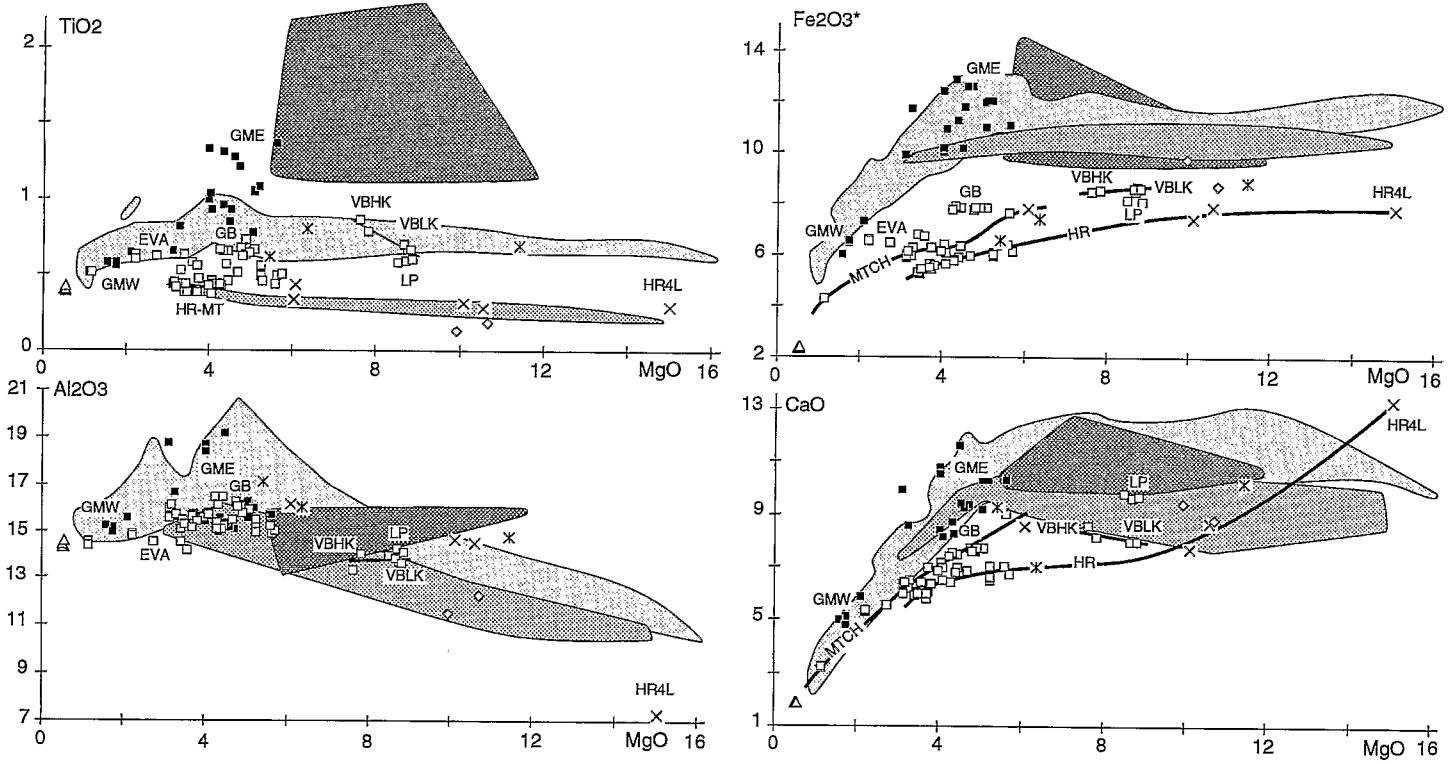

□ 1 HMA suite lavas

× 2 Matthew and Hunter inclusions; doleritic inclusions from both islands and one pyroxene cumulate from Hunter (HR 4L)

△ 3 Sodic rhyolites from the Hunter Ridge near 173°E

✳ 4 Basalt and basic andesites from the Hunter Ridge near 173°E

◇ 5 Boninites from the Hunter Ridge near 173°E

■ 6 IAB suite lavas

7 New Hebrides Central Chain

8 High-Ca boninites from the northern Tonga Ridge

9 BABB and MORB from the southernmost parts of the North Fiji Basin and from the Hunter Ridge

Fig. 6. Oxides% vs. MgO% diagrams; caption as for Fig. 5.

a distinct calc-alkaline trend, due to their higher MgO and lower FeO* contents at a given SiO_2 level, and an Fe-depletion trend with fractionation compared to the "normal" rocks; they are thus referred to as a "high-Mg" andesite suite, abbreviated herein to HMA.

It is worthwhile noting that true basalts ($<53\%$ SiO_2) are absent from the HMA lava suite. Inclusions in Matthew and Hunter lavas, some lavas from further east on the Hunter Ridge (including high-Mg andesites, rhyolites and boninites), and boninites from the northern Tonga Ridge, define similar compositional variations as the southern NH arc HMA suite, and it is likely that the parental magmas of this suite were boninitic according to the criteria of Crawford et al. (1989).

In Fig. 6, major- and minor-element oxides are plotted against MgO content. The IAB suite lavas show a slightly more restricted range of MgO (6 to 1%) in comparison with HMA rocks (9 to 1%), and the two suites are generally clearly separated on most of these plots. In general, IAB rocks plot in the fields defined by NH Central Chain rocks, whereas the HMA suite has higher SiO_2, Na_2O, K_2O, and lower TiO_2, $Fe_2O_3^*$, MnO, and CaO contents at a given MgO content. On the SiO_2 vs. MgO diagram, the field delineated by the HMA rocks overlaps the field of boninites from the northern Tonga Ridge. Nevertheless, on other diagrams (especially $Fe_2O_3^*$ and Na2O vs. MgO and to a lesser extent TiO_2 vs. MgO), these two fields are clearly separated.

Sampling carried out on each volcano is generally too poor to define individual trends on these major element binary diagrams. Nevertheless, analyses of IAB from Gemini East seamount define positive correlations between SiO_2 (51–54%), TiO_2 (0.9–1.4%), $Fe_2O_3^*$ (10–13%) and MnO (0.17–0.22%), all characteristic of a tholeiitic fractionation trend. However, compared to lavas of the Central Chain, basic andesites from Gemini East have unusually high TiO_2 contents, approaching those of the North Fiji Basin basalts. In contrast, the HMA lava suite, especially the andesites and dacites from Matthew and Hunter volcanoes, show very low TiO_2 contents (as low as 0.4% for HR), as previously noted by Gill (1981) and Maillet et al. (1986).

For each suite, SiO_2, Na2O, K_2O show clear negative correlations with MgO whereas TiO_2, $Fe_2O_3^*$, MnO and CaO are positively correlated with MgO content. Such correlations probably reflect fractional crystallization and/or magma mixing processes along two broad evolutionary trends originating from two distinct parental magmas. Basic andesites from La Perouse and Vauban seamounts represent the most primitive sampled lavas of the HMA series. However, complicating this simple scenario are large variations in TiO_2, MgO, K_2O and P_2O_5 contents of the Mg-rich basic andesites from Vauban, clearly transverse to the broad evolutionary trend of the HMA series, and requiring further explanation.

A second complicating factor centres on Gemini West seamount. This volcano is located well north of the 22°S dividing line between the IAB and HMA suites, and is close to the typically tholeiitic and IAB Gemini East seamount (Fig. 2). Most major element compositional features of Gemini West dacites are colinear with, or close to the trends for the HMA suite rocks (Figs. 6 and 7). In contrast, incompatible-trace-element and REE abundances in the Gemini West lavas are more characteristic of the IAB suite (Figs. 7 and 8, where SUB 1103 might represent in a broad sense a possible parental magma to the analysed Gemini West dacites), and indicate a strong decoupling of large ion lithophile elements (LILE) from major-element contents. This may reflect the fact that Gemini West sits 50 km closer to the east-dipping subducted slab than does its neighbour Gemini East seamount, so that magma generation processes as reflected in the major-element compositions for Gemini West are more akin to those occurring at shallower depth-to-slab distances, such as exist beneath the typically calc-alkaline to

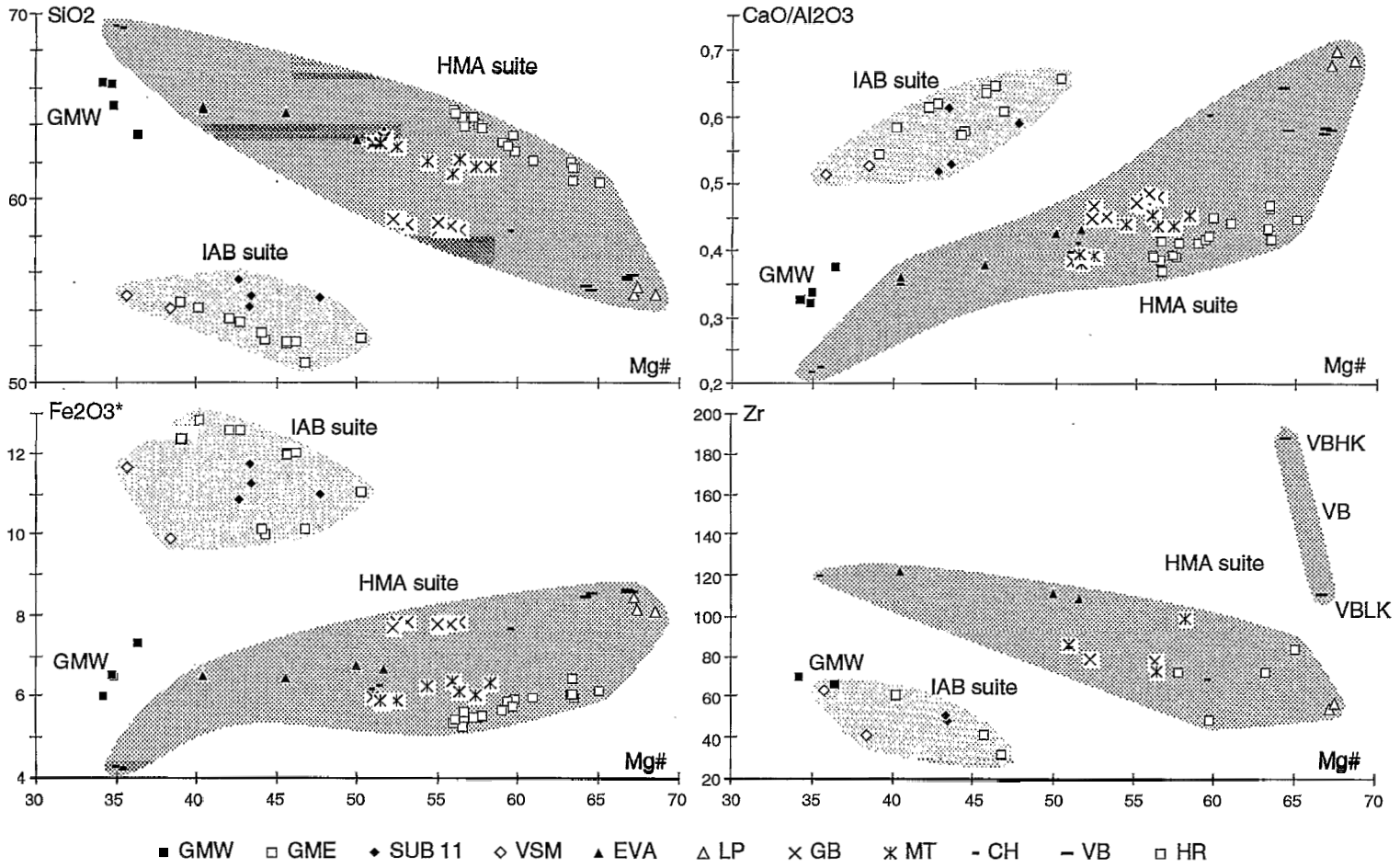

Fig. 7. $SiO_{2\%}$, $Fe_2O_3^*\%$, CaO/Al_2O_3 and Zr (ppm) vs. Mg# diagrams for individual volcanoes.

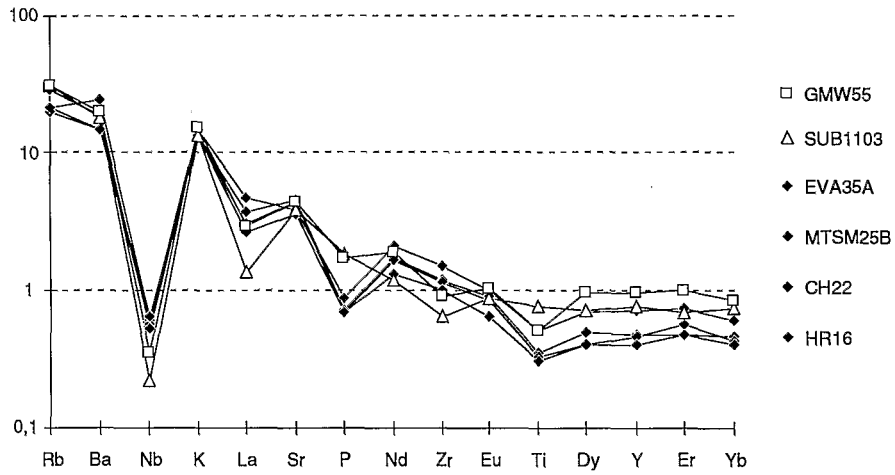

Fig. 8. N-MORB normalized incompatible-element abundance patterns for GMW 55 dacite and SUB 1103 basaltic andesite, both from the IAB suite, and for several acid andesites or dacites of the HMA suite (similar in SiO_2 content to GMW 55). Elements are ordered in sequence of decreasing incompatibility, from left to right, in oceanic basalts. This order and the concentrations in N-type MORB are taken from Sun and McDonough (1989).

boninitic HMA suite volcanoes. In contrast, the trace-element signatures are controlled to a significant degree by the nature of slab-derived fluids, and are similar for Gemini West and for the neighbouring IAB group volcanoes.

Variation diagrams for the compatible trace elements V, Cr and Ni vs. MgO and SiO_2% are given in Fig. 9. The two suites of lavas previously defined are clearly discriminated on the V vs. MgO diagram. The IAB series plots in the NH Central Chain lavas field, whereas the low-V content of the Mg-rich lavas is obvious, and parallels their low $Fe_2O_3^*$ contents, particularly Matthew, Charlotte and Hunter samples. On the Cr and Ni vs. SiO_2 diagrams, Gemini West, Gemini East, SUB 11 and Volsmar lavas again plot in the field of the NH Central Chain lavas. The HMA suite rocks at the low-SiO_2 end of their compositional spectrum overlap the field for northern Tonga Ridge boninites (Falloon and Crawford, 1991), Hunter Ridge boninites (Sigurdsson et al., 1993) and inclusions in Matthew and Hunter lavas (Maillet et al., 1986), but at SiO_2 contents $>57\%$, there is a suggestion of two trends, one defined by rocks from Hunter, the other by the remaining HMA suite rocks. This "boninitic" field shows large Cr and Ni variations (Cr=830 to 130 ppm; Ni=230 to 40 ppm) for a very narrow range of SiO_2 variation (SiO_2=54.5 to 57.6%), presumably reflecting olivine+Cr-spinel fractionation/accumulation with MgO buffered by clinopyroxene, the dominant mafic phenocryst phase in these rocks.

Except for some basaltic andesites from La Perouse and Vauban seamounts (and especially the K-rich basic andesites from Vauban), all the analyzed lavas are systematically lower in the more incompatible trace elements (Rb, Ba, La, Zr), at a given SiO_2 level, compared to recent lavas of the NH Central Chain volcanoes. In particular, all these lavas, without exception, have exceptionally low Ba contents, similar to those of MORB, back-arc basin basalts (BABB), or boninites (Fig. 10). For the less incompatible trace elements (Dy, Y, and Yb), IAB suite lavas plot in the field defined by the recent lavas of the NH Central Chain volcanoes, whereas HMA suite lavas (except for the high-K Vauban lavas) plot well beneath this field (Fig. 10).

N-MORB normalized element variation diagrams for the more mafic rocks studied are

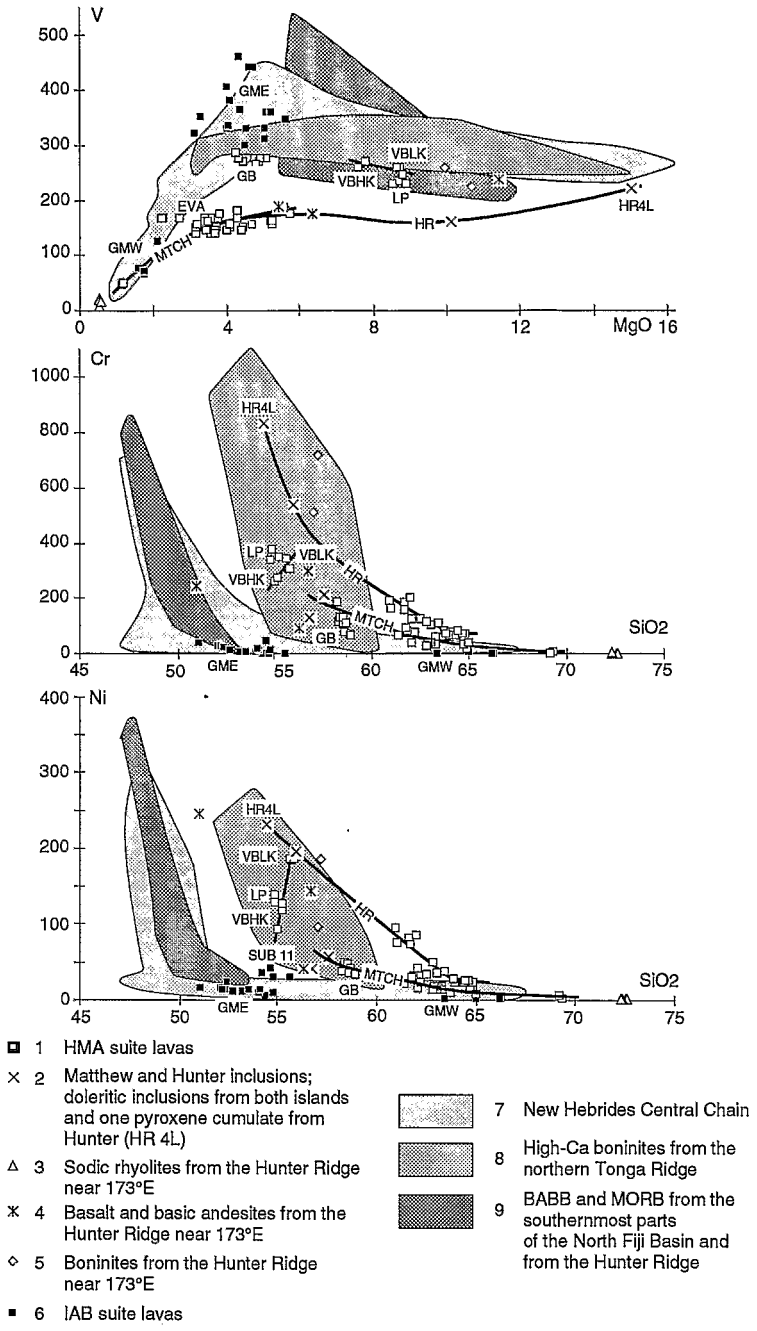

Fig. 9. V (ppm) vs. MgO% and Cr and Ni (ppm) vs. SiO_2% diagrams; caption as for Fig. 5.

given in Fig. 11. Characteristic arc-lava features of these patterns include the relative enrichment of LILE compared to high field strength elements (HFSE) and heavy REE, the pronounced negative Nb anomaly, the positive Sr anomaly, and levels of HFSE and HREE at or below N-MORB levels.

Within the IAB suite (Fig. 11A), the more magnesian ($41 < Mg\# < 49$) lavas show significant variation in the extent of enrichment of

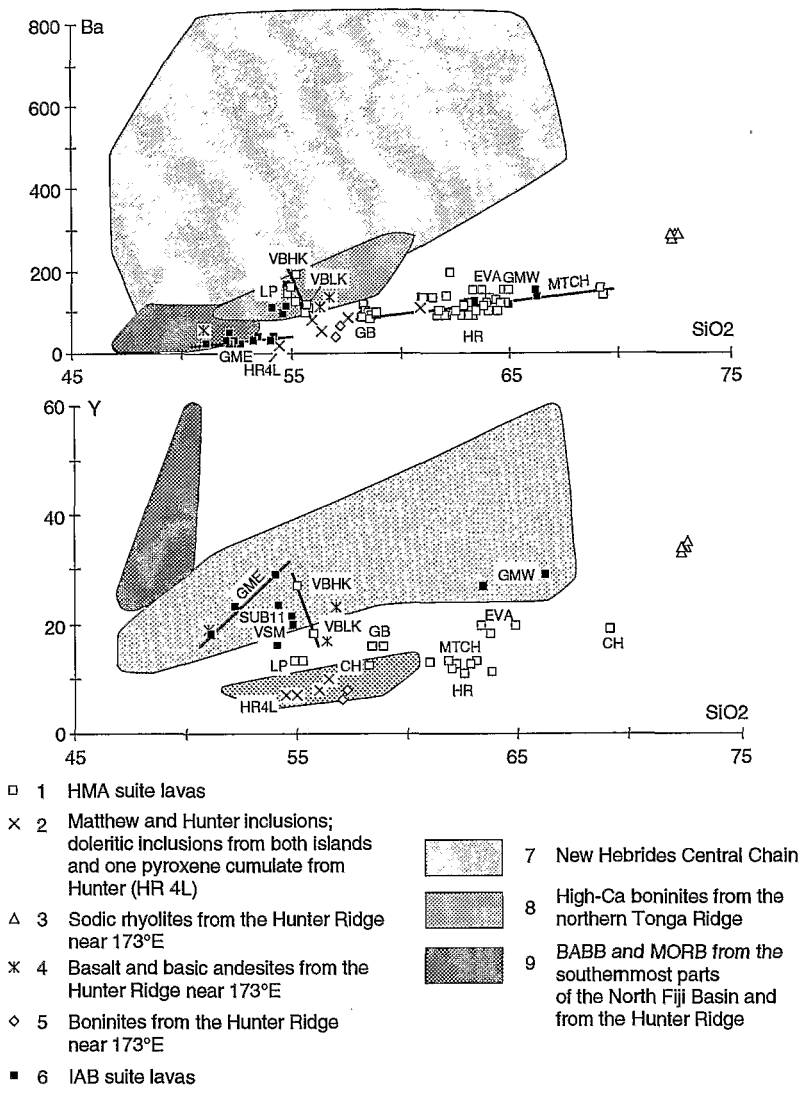

Fig. 10. Ba and Y (ppm) vs. $SiO_{2\%}$ diagrams; caption as for Fig. 5.

Rb, Ba and K, although the REE and HFSE show little variation. Except for slightly lower levels for the elements from P to Yb, element variation trends for basalts and basaltic andesites from Gemini East do not differ markedly from those of BABB from the southernmost North Fiji Basin, whereas the more K-rich basaltic andesites from SUB 11 (and possible parental magmas to the analysed Gemini West dacites) plot away from North Fiji Basin basalts field and fall in the field of NH Central Chain lavas. In contrast, the trace-element signatures for basaltic andesites from Volsmar seamount are very close to those for the "high-Mg" lavas (Fig. 11B). Although major-element abundances for Volsmar rocks are characteristic of the IAB suite (Fig. 8), Volsmar volcano is located close to the 22°S dividing line between the IAB and HMA suites (Fig. 2), which could explain trace-element abundances similar to those of the HMA suite lavas.

Excluding lavas from Vauban seamount, the more magnesian ($54 < Mg\# < 69$) lavas from the HMA suite define a fairly tight trend on

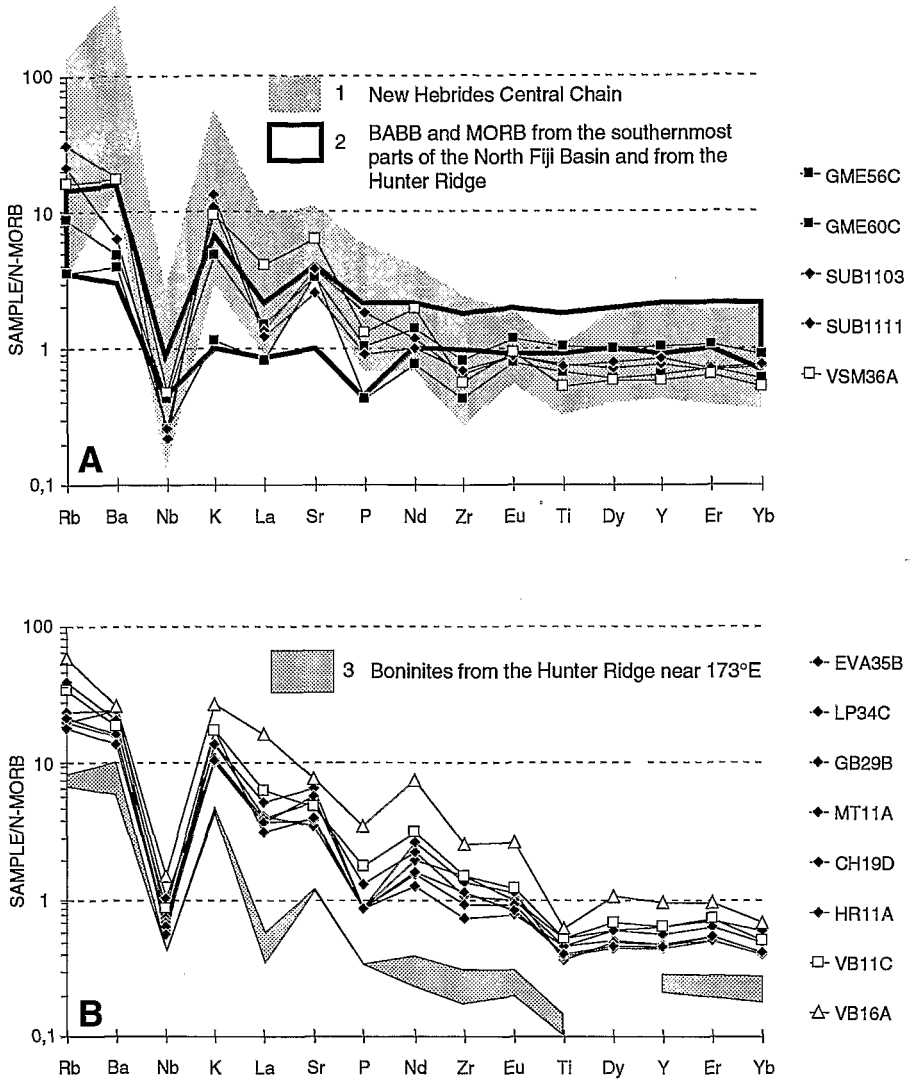

Fig. 11. N-MORB normalized incompatible-element abundance patterns for the more mafic rocks of the IAB (A) and HMA (B) suites (see caption of Fig. 8). For comparison: *1*: 204 unpublished analyses of recent New Hebrides Central Chain lavas (see caption of Fig. 5); *2*: from Eissen et al. (1991) and Sigurdsson et al. (1993); *3*: from Sigurdsson et al. (1993).

the N-MORB normalized element variation diagram (Fig. 11B). Although their element patterns are similar in shape to those of the IAB suite, they show notably lower levels of HREE and Ti, and higher levels of all elements more incompatible than Eu, including both Nb and Zr, than IAB group lavas. The two analyzed Vauban basaltic andesites, with Mg# values of 67 and 69, differ from the other HMA suite lavas in several respects. Firstly, neither shows a peak at Sr. Since these rocks contain similar modal abundances of plagioclase to the other mafic HMA suite samples plotted in Figure 11B, this difference cannot be attributed to plagioclase fractionation. Secondly, the HREE levels of the Vauban samples are higher than those of the other HMA suite lavas. Furthermore, the two Vauban rocks show markedly different levels of enrichment of the LREE, P, Zr and HREE, with those defined above on the

basis of their K_2O-SiO_2 relationships as being high-K having notably higher contents of these elements. Lastly, it is apparent that, excluding high-K Vauban lavas, the trends for the more magnesian lavas from the HMA suite broadly parallels from Rb to Ti the trend for the boninites from the Hunter Ridge (Fig. 11B).

In Fig. 12, Nb, La, Zr and Dy contents, and La/Dy, are plotted for all analyzed samples, from northwest to southeast, according to their position along the southernmost NH arc. These plots effectively demonstrate the significant compositional differences between the IAB and the HMA lava suites.

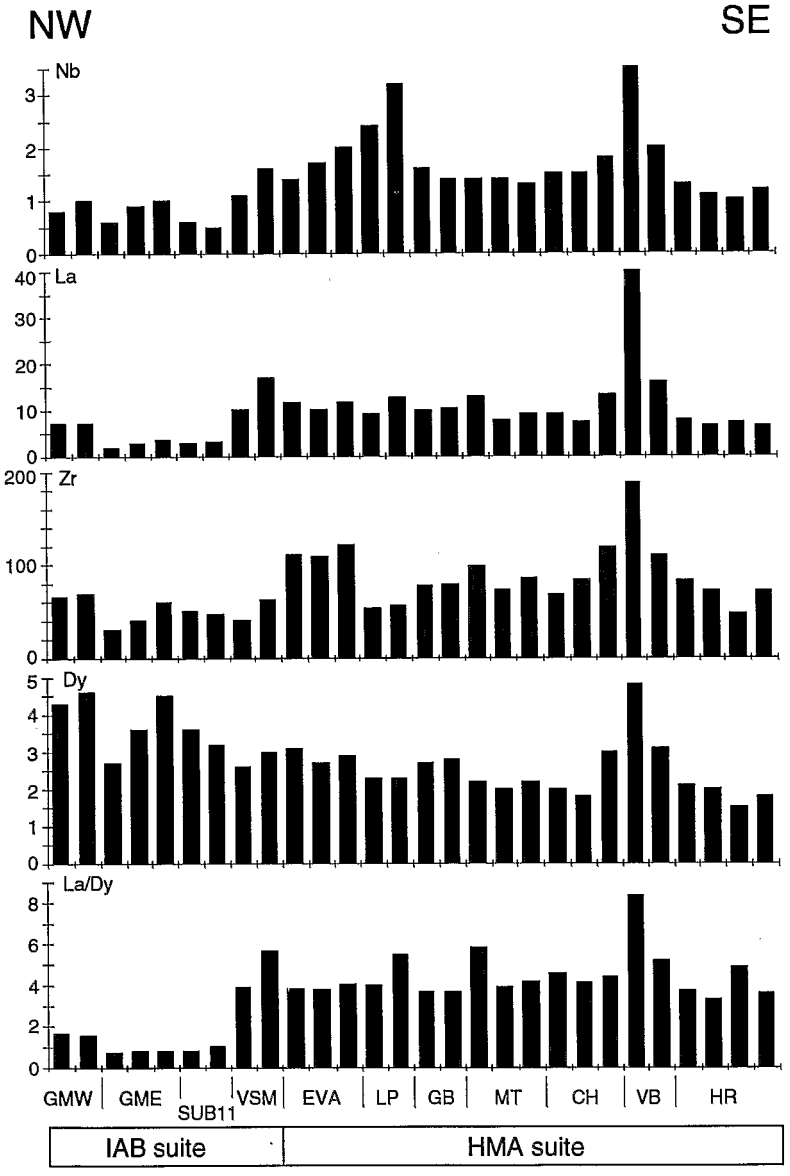

Fig. 12. Nb, La, Zr and Dy contents (in ppm), and La/Dy ratio, plotted for all analyzed samples, from northwest to southeast, according to their position along the southern NH arc termination.

We have begun a more detailed petrological and isotopic study of the lavas described here, which will be published elsewhere.

5. Discussion

The major- and trace-element variation trends described above can be considered, to a first approximation, as having been produced by fractional crystallization processes operating on two spatially distinct arc magmatic suites. As these two magmatic suites, IAB and HMA, appear to occur in two distinct tectonic settings, magmatic and tectonic processes are closely linked at the southern termination of the NH arc. In this perspective, the magmatic evolution of the IAB suite is probably governed by petrogenetic processes similar to those occurring in the main part of the NH arc (Crawford et al., 1988; Eggins, 1989; Eggins, 1993), whereas the HMA suite has a more atypical origin and evolution.

Magmas similar to the most mafic lavas from La Perouse and Vauban seamounts are probably parental to the HMA suite, and have some compositional affinities to high-Ca boninites (Crawford et al., 1989). Interestingly, true high-Ca boninites have been dredged only 100 km to the east of Hunter island, in the area where the N–S North Fiji Basin spreading axis abuts the Hunter Fracture Zone (Crawford and Eggins, 1991; Sigurdsson et al., 1993). In such a complex tectonic setting, with a spreading axis propagating into an intra-oceanic arc, in an area dominated by transform plate motion (Maillet et al., 1989), boninite generation occurs by melting of a refractory hydrated mantle at a shallow level under the Hunter Ridge, the necessary extra heat being supplied by the rising diapirs of the intersecting spreading axis. Generation of boninites in this area was predicted by Crawford et al. (1989) and, in a similar tectonic setting at the northern end of the Tonga arc, high-Ca boninites are also known (Sharaskin et al., 1983; Danyushevsky and Sobolev, 1987; Falloon et al., 1987, 1989; Falloon and Crawford, 1991). Major-element concentrations of the mafic andesites from La Perouse and Vauban seamounts, boninites from the northern end of the Tonga arc, boninites from the Hunter Ridge, and doleritic inclusions from Matthew and Hunter islands (Maillet et al., 1986) are compositionally similar (Table 3), with slight differences for TiO_2, alkalies and P_2O_5.

Doleritic inclusions are common in Mg-rich acid andesites of Matthew and Hunter islands (up to 1–2% by volume). These generally have acicular mineral morphologies and a glassy,

TABLE 3

Major-element compositions of boninites from the northern Tonga Ridge (bon. 1 = 3-53-IV, 3-22-IV and 3-28-IV samples with MgO ≈ 8%, bon. 2 = 3-21-II, 3-51-II, 3-25-III, and 3-24-V samples with MgO ≈ 10–11%; Falloon and Crawford, 1991), boninites from the Hunter Ridge (105.1 and 2 in Sigurdsson et al., 1993), doleritic inclusions in Matthew and Hunter acid andesites (MT 35A and B, HR 4M and HR 8G in Maillet et al., 1986) and basaltic andesites from LP and VB seamounts (this study). All data with total iron as Fe_2O_3 and recalculated to 100% volatile free

	NT bon. 1	NT bon. 2	HRFZ bon.	HR dol. incl.	MT dol. incl.	LP	VBLK	VBHK
SiO2	53.8-56.9	53.4-58.6	57.1-57.3	54.7-56.0	56.8-57.6	54.9-55.3	55.7-55.9	55.1-55.2
TiO2	0.27-0.29	0.23-0.30	0.13-0.18	0.28-0.31	0.34-0.44	0.58-0.59	0.66-0.69	0.78-0.86
Al2O3	13.1-14.7	10.9-12.7	11.5-12.3	14.5-14.6	16.1	13.9-14.2	13.6-13.8	13.3-14.0
Fe2O3*	10.1-11.0	9.7-10.9	8.7-9.7	7.4-7.9	7.6-7.8	8.1-8.4	8.5-8.6	8.4-8.5
MnO	0.17-0.19	0.16-0.18	0.15-0.17	0.14-0.15	0.12-0.14	0.15	0.14	0.14
MgO	7.7-8.1	10.3-11.0	10.0-10.7	10.1-10.6	6.0-6.1	8.5-8.9	8.7-8.8	7.6-7.8
CaO	9.4-10.6	7.7-10.4	8.8-9.4	7.7-8.7	8.5-8.6	9.6-9.8	7.9-8.0	8.1-8.5
Na2O	1.3-1.6	1.4-1.6	1.5-1.6	2.7-3.1	3.0-3.1	2.5-2.6	3.0	3.2-3.3
K2O	0.40-0.53	0.44-0.57	0.32-0.36	0.50	0.60-1.00	0.74-0.94	1.24-1.28	1.92-2.03
P2O5	0.04-0.06	0.03-0.07	0.04	0.11		0.10-0.12	0.20-0.30	0.41-0.60
Mg#	0.58-0.61	0.65-0.69	0.67-0.71	0.73	0.61	0.67-0.69	0.67	0.64-0.65
CaO/Al2O3	0.72	0.71-0.82	0.72-0.82	0.53-0.60	0.53	0.68-0.70	0.58	0.58-0.64

vesicle-rich matrix, suggestive of a quench origin. They may represent quenched blobs of near-parental boninitic high-Mg andesite magma incorporated into the acid andesite host magma prior to eruption. As suggested by Maillet et al. (1986), and shown in Figs. 6 and 8, inclusions and host-lavas are almost certainly comagmatic. Intra-flow inhomogeneities and banding in Matthew and Hunter andesites suggest that even if fractional crystallization is the main differentiation process, mixing of cogenetic mafic and more evolved magmas is certainly frequent on Matthew and Hunter. The same combination of fractional crystallization and magma mixing might occur along the whole southern termination of the arc, and is presently being tested by melt inclusion studies.

At the southern termination of the New Hebrides arc, dominated as it has been over the last few Ma by fast transform motions, both the low magmatic production rates for these volcanoes, and the unusual broadly boninitic affinities of the arc volcanism may be due to a combination of a downgoing slab torn by hinge zones, unusually small depth-to-slab distances for the volcanoes, and an unusually hot regional upper mantle due to diapirs supplying the intersecting back-arc spreading axis. The ongoing collision between the Loyalty Ridge and the arc may also be partly responsible for these unusual magmatic characteristics, as presently only a very small amount of convergence occurs along the southernmost segment of the trench.

Acknowledgements

VOLSMAR and GEMINI cruises were supported by Département TOA of ORSTOM (Paris). We are deeply indebted to P. Furic, captain of the R.V. "Alis" (ORSTOM), as well as to the whole crew. We acknowledge all the scientists and scuba-divers who participated in this cruises. We also express our thanks to the crews of the R.V. "Nadir" and "Nautile" (IFREMER) and to the scientists and technicians involved in the SUBPSO 1 cruise (ORSTOM), with special mention to B. Pelletier for the skillful job done aboard Nautile during the SUBPSO 11 dive. Thoughtful reviews by A. Ewart and J.A. Gamble have resulted in a much improved manuscript.

References

Andrews, J.E., Packham, G. et al., 1975. Sites 285 and 286. In: J.E. Andrews, G. Packham et al., Initial Reports of the Deep Sea Drilling Project. U.S. Government Printing Office, Washington, 30: 27–131.

Auzende, J.M., Lafoy, Y. and Marsset, B., 1988. Recent geodynamic evolution of the North Fiji Basin (Southwest Pacific). Geology, 16: 925–929.

Charvis, P. and Pelletier, B., 1989. The northern New Hebrides back-arc troughs: history and relation with the North Fiji Basin. Tectonophysics, 170: 259–277.

Chase, T.E. and Seekins, B.A., 1988. Submarine topography of the Vanuatu and southeastern Solomon islands regions. In: H.G. Greene and F.L. Wong (Editors), Geology and Offshore Resources of Pacific Island Arcs — Vanuatu region. Circum Pacific Council for Energy and Mineral Resources, Earth Sci. Ser. 8, Houston, Texas, p. 35+2 maps.

Collot, J.Y., 1989. Obduction et collision: exemples de la Nouvelle-Calédonie et de la zone de subduction des Nouvelles-Hébrides. Thèse de Doctorat d'Etat, Université de Paris XI, 476 pp.

Collot, J.Y., Daniel, J. and Burne, R.V., 1985. Recent tectonics associated with the subduction/collision of the d'Entrecasteaux Zone in the central New Hebrides. Tectonophysics, 112: 325–356.

Collot, J.Y., Lallemand, S., Pelletier, B., Eissen, J.P., Glaçon, G., Fisher, M.A., Greene, H.G., Boulin, J., Daniel, J. and Monzier, M., 1992. Geology of the D'Entrecasteaux–New Hebrides island-arc collision zone: results from a deep-sea submersible survey. Tectonophysics, 212: 213–241.

Collot, J.Y., Missegue, F. and Malahoff, A., 1982. Anomalies gravimétriques et structure de la croûte dans la région de la Nouvelle-Calédonie: enracinement des péridotites. In: Equipe de Géologie-Géophysique du Centre ORSTOM de Nouméa (Editor), Contribution à l'étude géodynamique du Sud-Ouest Pacifique. Trav. Doc. ORSTOM, Paris, 147: 549–564.

Collot, J.Y., Pelletier, B., Boulin, J., Daniel, J., Eissen, J.P., Fisher, M.A., Greene, H.G., Lallemand, S. and Monzier, M., 1989. Premiers résultats des plongées de la campagne SUBPSO 1 dans la zone de collision des rides d'Entrecasteaux et de l'arc des Nouvelles-Hébrides. C.R. Acad. Sci. Paris, 309, II: 1947–1954.

Crawford, A.J. and Eggins, S.M., 1991. Boninites from the North Fiji Basin–Hunter "Fracture Zone". Abstract, STARMER Symposium, 7–11 february 1991, ORSTOM Center, Noumea, New Caledonia.

Crawford, A.J., Greene, H.G. and Exon, N.F., 1988. Geology, petrology and geochemistry of submarine volcanoes from around Epi Island, New Hebrides Island Arc. In: H.G. Greene and F.L. Wong (Editors), Geology and Offshore Resources of Pacific Island Arcs — Vanuatu region. Circum Pacific Council for Energy and Mineral Resources, Earth Sci. Ser. 8, Houston, Texas, pp. 301–327.

Crawford, A.J., Falloon, T.J. and Green, D.H., 1989. Classification, petrogenesis and tectonic setting of boninites. In: A.J. Crawford (Editor), Boninites. Unwin Hyman, London, UK, pp. 1–49.

Daniel, J., Collot, J.Y., Monzier, M., Pelletier, B., Butscher, J., Deplus, C., Dubois, J., Gérard, M., Maillet, P., Monjaret, M.C., Récy, J., Renard, V., Rigolot, P. and Temakon, J., 1986. Subduction et collisions le long de l'arc des Nouvelles-Hébrides (Vanuatu): résultats préliminaires de la campagne SEAPSO (Leg I). C.R. Acad. Sc. Paris, 303, II, 9: 805–810.

Danyushevsky, L.V. and Sobolev, A.V., 1987. New data on the petrology of boninites in Tonga. Akad. Nauk. USSR, Geol. Geophys., 12: 100–103.

Davey, F.J., 1982. The structure of the south Fiji basin. Tectonophysics, 87: 185–241.

Dziewonski, A.M. and Woodhouse, J.H., 1983. An experiment in systematic of global seismicity: centroid-moment tensor solutions for 201 moderate and large earthquakes of 1981. J. Geophys. Res., 88(B4): 3247–3271.

Dziewonski, A.M., Friedman, A., Giardini, D. and Woodhouse, J.H., 1983a. Global seismicity of 1982: centroid-moment tensor solutions for 308 earthquakes. Phys. Earth Planet. Inter., 33: 76–90.

Dziewonski, A.M., Franzen, J.E. and Woodhouse, J.H., 1983b. Centroid-moment tensor solutions for April–June, 1983. Phys. Earth Planet. Inter., 33: 243–249.

Dziewonski, A.M., Franzen, J.E. and Woodhouse, J.H., 1984a. Centroid-moment tensor solutions for July–September, 1983. Phys. Earth Planet. Inter., 34: 1–8.

Dziewonski, A.M., Franzen, J.E. and Woodhouse, J.H., 1984b. Centroid-moment tensor solutions for January–March, 1984. Phys. Earth Planet. Inter., 34: 209–219.

Dziewonski, A.M., Franzen, J.E. and Woodhouse, J.H., 1985. Centroid-moment tensor solutions for January–March, 1985. Phys. Earth Planet. Inter., 40: 249–258.

Dziewonski, A.M., Franzen, J.E. and Woodhouse, J.H., 1986. Centroid-moment tensor solutions for July–September, 1985. Phys. Earth Planet. Inter., 42: 205–214.

Dziewonski, A.M., Ekström, G., Franzen, J.E. and Woodhouse, J.H., 1987a. Centroid-moment tensor solutions for April–June, 1986. Phys. Earth Planet. Inter., 45: 229–239.

Dziewonski, A.M., Ekström, G., Franzen, J.E. and Woodhouse, J.H., 1987b. Global seismicity of 1977: centroid-moment tensor solutions for 471 earthquakes. Phys. Earth Planet. Inter., 45: 11–36.

Dziewonski, A.M., Ekström, G., Franzen, J.E. and Woodhouse, J.H., 1987c. Global seismicity of 1978: centroid-moment tensor solutions for 512 earthquakes. Phys. Earth Planet. Inter., 46: 316–342.

Dziewonski, A.M., Ekström, G., Franzen, J.E. and Woodhouse, J.H., 1987d. Global seismicity of 1979: centroid-moment tensor solutions for 524 earthquakes. Phys. Earth Planet. Inter., 48: 18–46.

Dziewonski, A.M., Ekström, G., Franzen, J.E. and Woodhouse, J.H., 1988a. Global seismicity of 1980: centroid-moment tensor solutions for 515 earthquakes. Phys. Earth Planet. Inter., 50: 127–154.

Dziewonski, A.M., Ekström, G., Franzen, J.E. and Woodhouse, J.H., 1988b. Global seismicity of 1981: centroid-moment tensor solutions for 542 earthquakes. Phys. Earth Planet. Inter., 50: 155–182.

Dziewonski, A.M., Ekström, G., Franzen, J.E. and Woodhouse, J.H., 1988c. Global seismicity of 1982 and 1983: additional centroid-moment tensor solutions for 533 earthquakes. Phys. Earth Planet. Inter., 53: 17–45.

Eggins, S.M., 1989. The origin of primitive ocean island and island arc basalts. PhD Thesis (unpublished), University of Tasmania, 402pp.

Eggins, S.M., 1993. Origin and differentiation of primitve arc lavas, Aoba (Ambae) Island, Vanuatu. Contrib. Mineral. Petrol., 114: 79–100.

Eissen, J.-P., Lefèvre, C., Maillet, P., Morvan, G. and Nohara, M., 1991. Petrology and geochemistry of the central North Fiji Basin spreading centre (Southwest Pacific) between 16°S and 22°S. Mar. Geol., 98: 201–239.

Falloon, T.J. and Crawford, A.J., 1991. The petrogenesis of high-calcium boninite lavas dredged from the northern Tonga Ridge. Earth Planet. Sci. Lett., 102: 375–394.

Falloon, T.J., Green, D.H. and Crawford, A.J., 1987. Dredged igneous rocks from the northern termination of the Tofua magmatic arc, Tonga and adjacent Lau Basin. Aust. J. Earth Sci., 34: 487–506.

Falloon, T.J., Green, D.H. and McCulloch, M.T., 1989. Petrogenesis of "high-Mg" and associated lavas from the north Tonga trench. In: A.J. Crawford (Editor), Boninites. Unwin Hyman, London, pp. 357–395.

Falvey, D.A., 1978. Analysis of paleomagnetic data from the New Hebrides. Aust. Soc. Explor. Geophys. Bull., 9: 117–123.

Falvey, D.A. and Greene, H.G., 1988. Origin and evolution of the sedimentary basins of the New Hebrides arc. In: H.G. Greene and F.L. Wong (Editors), Geology and Offshore Resources of Pacific Island Arcs —

Vanuatu region. Circum Pacific Council for Energy and Mineral Resources, Earth Sci. Ser. 8, Houston, Texas, pp. 413–442.

Giardini, D., Dziewonski, A.M. and Woodhouse, J.H., 1985. Centroid-moment tensor solutions for 113 large earthquakes in 1977–1980. Phys. Earth Planet. Inter., 40: 259–272.

Gill, J.B., 1981. Orogenic Andesites and Plate Tectonics. Minerals and Rocks 16, Springer-Verlag, Berlin-Heidelberg-New York, 390 pp.

Greene, H.G., Collot, J.-Y. and Fisher, M.A., in press. Neogene tectonic evolution of the New Hebrides Island Arc — a review incorporating ODP drilling results. In: H.G. Greene, J.-Y. Collot, L.B. Stokking et al. (in press). Proc. ODP, Sci. Results, 134: College Station, TX (Ocean Drilling Program).

Greene, H.G., Macfarlane, A. and Wong, F.L., 1988. Geology and offshore resources of Vanuatu — Introduction and summary. In: H.G. Greene and F.L. Wong (Editors), Geology and Offshore Resources of Pacific Island Arcs — Vanuatu region. Circum Pacific Council for Energy and Mineral Resources, Earth Sci. Ser. 8, Houston, Texas, pp. 1–25.

Katz, H.R., 1988. Offshore geology of Vanuatu — Previous work. In: H.G. Greene and F.L. Wong (Editors), Geology and Offshore Resources of Pacific Island Arcs — Vanuatu region. Circum Pacific Council for Energy and Mineral Resources, Earth Sci. Ser. 8, Houston, Texas, pp. 93–122.

Kroenke, L.W., Jouannic, C. and Woodward, P., (compilers), 1983. Bathymetry of the Southwest Pacific, scale 1:6 442 192 at 0°, 2 sheets, Mercator Projection, Suva, Fiji, UN ESCAP, CCOP/SOPAC Technical Secretariat.

Lafoy, Y., Auzende, J.M., Ruellan, E., Huchon, P. and Honza, E., 1990. The 16°40'S triple junction in the North Fiji Basin (SW Pacific). Mar. Geophys. Res., 12: 285–296.

Louat, R. and Pelletier, B., 1989. Seismotectonics and present-day relative plate motions in the New Hebrides–North Fiji Basin region. Tectonophysics, 167: 41–55.

Louat, R., Hamburger, M. and Monzier, M., 1988. Shallow and intermediate-depth seismicity in the New Hebrides arc: constraints on the subduction process. In: H.G. Greene and F.L. Wong (Editors), Geology and Offshore Resources of Pacific Island Arcs—Vanuatu region. Circum Pacific Council for Energy and Mineral Resources, Earth Sci. Ser. 8, Houston, Texas, pp. 329–356.

Macfarlane, A., Carney, J., Crawford, A.J. and Greene, H.G., 1988. Vanuatu — A review of the onshore geology. In: H.G. Greene and F.L. Wong (Editors), Geology and Offshore Resources of Pacific Island Arcs—Vanuatu region. Circum Pacific Council for Energy and Mineral Resources, Earth Sci. Ser. 8, Houston, Texas, pp. 45–91.

Maillet, P., Monzier, M., Sélo, M. and Storzer, D., 1983. The d'Entrecasteaux Zone (Southwest Pacific). A petrological and geochronological reappraisal. Mar. Geol., 53: 179–197.

Maillet, P., Monzier, M. and Lefèvre, C., 1986. Petrology of Matthew and Hunter volcanoes, south New Hebrides island arc (southwest Pacific). J. Volcanol. Geotherm. Res., 30: 1–27.

Maillet, P., Monzier, M., Eissen, J.P. and Louat, R., 1989. Geodynamics of an arc-ridge junction: the case of the New Hebrides Arc / North Fiji Basin. Tectonophysics, 165: 251–268.

Miyashiro, A., 1974. Volcanic rocks series in island arcs and active continental margins. Am. J. Sci., 274: 321–355.

Monjaret, M.C., 1989. Le magmatisme des fossés à l'arrière de l'arc des Nouvelles-Hébrides (Vanuatu). Thesis, Univ. Bretagne Occidentale, Brest, 275 pp.

Monjaret, M.C., Bellon, H. and Maillet, P., 1991. Magmatism of the troughs behind the New Hebrides island arc (RV Jean Charcot SEAPSO 2 cruise): K-Ar geochronology and petrology. J. Volcanol. Geotherm. Res., 46: 265–280.

Monzier, M., 1991. The boninitic trend of the southern termination of the New Hebrides island arc (SW Pacific). Poster, STARMER Symposium, 7–11 february 1991, ORSTOM Center, Noumea, New Caledonia.

Monzier, M., Maillet, P., Foyo Herrera, J., Louat, R., Missègue, F. and Pontoise, B., 1984. The termination of the southern New Hebrides subduction zone (southwestern Pacific). Tectonophysics, 101: 177–184.

Monzier, M., Boulin, J., Collot, J.Y., Daniel, J., Lallemand, S. and Pelletier, B., 1989. Premiers résultats des plongées NAUTILE de la campagne SUBPSO I sur la zone de collision "ride des Loyauté / arc des Nouvelles-Hébrides" (Sud-Ouest Pacifique). C.R. Acad. Sci. Paris, 309, II: 2069–2076.

Monzier, M., Daniel, J. and Maillet, P., 1990. La collision "ride des Loyauté / arc des Nouvelles-Hébrides" (Pacifique Sud-Ouest). Oceanol. Acta, Actes du colloque Tour du Monde Jean Charcot, 2–3 mars 1989, Paris, Vol. Spéc., 10: 43–56.

Monzier, M., Maillet, P. and Dupont, J., 1992. Carte bathymétrique des parties méridionales de l'arc insulaire des Nouvelles-Hébrides et du bassin Nord-Fidjien. Institut Français de Recherche Scientifique pour le Développement en Coopération (ORSTOM), Paris.

Monzier, M., Pelletier, B., Daniel, J., Bellon, H., Glaçon, G., Montaggioni, L., Boulin, J., Collot, J.Y., Eissen, J.P. and Lallemand, S., in prep.. Nautile deep dives on the "Loyalty islands ridge / New Hebrides Island arc" collision zone (SW Pacific) and their contribution to the regional geology.

Pearce, J.A., 1983. The role of sub-continental lithosphere in magma genesis at destructive plate margins. In: C.J. Hawkesworth and M.J. Norry (Editors), Continental Basalts and Mantle Xenoliths. Shiva, Nantwich, pp. 230–249.

Pelletier, B., Missegue, F., Lafoy, Y., Mollard, L., Decourt, R., Dupont, J., Join, Y., Perrier, J. and Recy, J., 1993. Extrémités nord du bassin Nord-Fidjien et des fossés arrière-arc des Nouvelles-Hébrides: morphostructure et signature magnétique. C.R. Acad. Sci. Paris, 316, II: 637–644.

Récy, J., Charvis, Ph., Ruellan, E., Monjaret, M.C., Gérard, M., Auclair, G., Baldassari, C., Boirat, J.M., Brown, G.R., Butscher, J., Collot, J.Y., Daniel, J., Louat, R., Monzier, M. and Pontoise, B., 1986. Tectonique et volcanisme sous-marin à l'arrière de l'arc des Nouvelles-Hébrides (Vanuatu, Pacifique sud-ouest): résultats préliminaires de la campagne SEAPSO Leg II du N/O Jean Charcot. C.R. Acad. Sc. Paris, 303, II, 8: 685–690.

Récy, J., Pelletier, B., Charvis, Ph., Gérard, M., Monjaret, M.C. and Maillet, P., 1990. Structure, âge et origine des fossés arrière-arc des Nouvelles-Hébrides (Sud-Ouest Pacifique). Oceanolog. Acta, Actes du colloque Tour du Monde Jean Charcot, 2–3 mars 1989, Paris, Vol. Spéc., 10: 165–182.

Sharaskin, A. Ya., Pustchin, I.K., Zlobin, S.K. and Kolesov, G.M., 1983. Two ophiolite sequences from the basement of the northern Tonga arc. Ofioliti, 8: 411–430.

Sigurdsson, I.A., Kamenetsky, V.S., Crawford, A.J., Eggins, S.M. and Zlobin, S.K., 1993. Primitive island arc and oceanic lavas from the Hunter Ridge – Hunter Fracture Zone: Evidence from glass, olivine and spinel compositions. Mineral. Petrol. 47: 149–170.

Sun, S.-S. and McDonough, W.I., 1989. Chemical and isotopic systematics of oceanic basalts: implications for mantle composition and processes. In: A.D. Saunders and M.J. Norry (Editors), Magmatism in the Ocean Basins. Geol. Soc. Spec. Publ., 42: 313–345.

U.S. Geological Survey — National Earthquake Information Center (USGS-NEIC), 1987 to March 1990. Preliminary Determinations of Epicenters, monthly listing. Denver, CO.

Weissel, J.K., Watts, A.B. and Lapouille, A., 1982. Evidence for late Paleocene to late Eocene seafloor in the southern New Hebrides basin. Tectonophysics, 87: 243–251.